EXPLORING HYPOXIA SIGNALING REGULATION BY KERATIN 8 IN THE COLON

Frank Weckström

41267

fweckstr@abo.fi

Master's thesis, 40 ECTS, CB00BR56

Cell biology, Faculty of Science and Engineering, Åbo Akademi University

Supervisors:

Associate Professor, Docent Diana Toivola

Master of Science, Carl-Gustaf Stenvall

2022

Frank Weckström

EXPLORING HYPOXIA SIGNALING REGULATION BY KERATIN 8 IN THE COLON

Department of Biosciences, Åbo Akademi University

ABSTRACT

The innermost lining of the colon is covered with rapidly renewing epithelial cells expressing a composition of specific keratins. Keratins are part of the cell specific cytoskeletal group called intermediate filaments (IF) and are mainly located in epithelial cells. They are dynamic proteins assembling into filaments in the cytoplasm to provide structural support and resistance against different stress stimuli. It has also been shown that Keratin 8 (K8) loss influences, among other things, the hypoxic pathway, a pathway activated in hypoxic (low oxygen) conditions to save the cells from damage and death.

The aim of this study was to investigate and determine how K8 is involved in the regulation of the hypoxia pathway in the colon using K8-deficient cell- and mouse models. Our results indicate that K8 is in a complex with the hypoxia pathway transcription factor, hypoxia-inducible factor 1α (HIF-1α), and the loss of K8 can lead to an increase of HIF-1α translocation to the nucleus during normoxic (normal oxygen) conditions, however, not during hypoxia. Furthermore, we have shown *in vivo*, *in vitro* and *ex vivo* that K8 loss leads to increased levels of HIF-1α, not as a result of inflammation, but likely as a consequence of lost interaction with the PI3K/Akt/mTOR pathway. Interestingly, *in vivo* analysis of HIF-1α target genes mRNA showed no significant differences between $K8^{-/-}$ and $K8^{+/+}$ models, indicating that the transcriptional activity of HIF-1α is suppressed. Lastly, we determined with *in vitro* experiments that keratins are not upregulated during acute hypoxic stress. In conclusion, K8 may modulate the hypoxia signaling by suppressing the translation and nuclear translocation of HIF-1α.

Keywords: *Colon, HIF-1α, Hypoxia pathway, Intermediate filaments, Keratins*

TABLE OF CONTENT

ABBREVIATIONS

Akt	Protein kinase B
AOM	Azoxymethane
ARNT	Aryl hydrocarbon receptor nuclear translocator
ARD-1	Arrest-defect-1
Bcl2	B-cell lymphoma 2
BMP signaling	Bone morphogenetic protein signaling
BSA	Bovine serum albumin
CBP	CREB- binding protein
$CoCl_2$	Cobalt chloride
DMOG	Dimethyloxalylglycine
DTT	Dithiotreitol
EDTA	Ethylenediaminetetraacetic acid
ERK	Extracellular signal-regulated kinase
eIF-4E	Eukaryotic translation initiation factor 4E
FAK	Focal-adhesion kinase-1
FIH-1	Factor inhibiting HIF-1
HIF-1α	Hypoxia-inducible factor 1α
HOX	Hypoxia
IBD	Inflammatory bowel disease
IF	Intermediate filaments
MDM2	Mouse double minute 2
MHCII	Major histocompatibility complex 2
MNK	MAP kinase-interacting kinase
mTOR	Mammalian target of rapamycin
NOX	Normoxia
PBS	Phosphate buffered saline
PBS-T	PBS- 0.2 % Tween
PFA	paraformaldehyde
PHD-2	Prolyl hydroxylase domain-2
PI	Protease inhibitor
PI3K	Phosphoinositide 3-kinase
PKC	Protein kinase C

PMSF	Phenylmethylsulfonyl fluoride
PVDF	Polyvinylidene difluoride
RACK1	Receptor for activated protein kinase C
RT	Room temperature
SDS	Sodium dodecyl sulfate
SDS-PAGE	SDS- Polyacrylamide gel electrophoresis
Src	Src kinase
S6K	S6 kinase
Th2	T-helper 2
TNFR2	Tumor necrosis factor receptor 2
VEGF	Vascular endothelial growth factor
VHL	Von Hippel-Lindau
4E-BP1	4E- Binding protein 1

1 INTRODUCTION

All cells consist of a rigid network of cytoskeletal proteins assisting the cell in various cellular processes such as structural support, movement, and transportation. The cytoskeleton is divided into three main groups: microfilaments, microtubules, and intermediate filaments. The intermediate filaments are very flexible, dynamic and nearly insoluble proteins that create filaments reaching across the cytosol and connecting to other cytoskeletons (Omary, 2009; Fletcher, Mullins, 2010). In contrast to microfilaments and microtubules, the intermediate filaments are divided into six types, which are expressed cell and tissue specifically. This thesis will focus on the Type I and Type II intermediate filaments called keratins (K).

The colon is part of the 1.5-meter-long large intestine located in the final part of the gastrointestinal tract, and has the function of extracting the last nutrients, water, vitamins, and minerals from the chyme. Located in the innermost layer of the colon is the epithelium consisting of rapidly renewing crypts. It has the function of absorption, producing mucus, signaling (e.g, gut to brain) and together with the gut bacterial ecosystem it creates a wall defending against pathogens (Garrett, Gordon & Glimcher, 2010; Caballero, Finglas & Toldrá, 2015). The epithelium is rich in Type I and Type II intermediate filaments, i.e., keratins. The main keratins in the colon (K8, K18, K19, K20) create a network of scaffolds, which protect the cells from mechanical and chemical stress, as well as participate in signaling and compartmentalization (Pallari, Eriksson, 2006; Polari et al., 2020). The importance of keratins in the colon has been shown by studies where K8 loss in mice causes hyperproliferation, colitis and diarrhea (Baribault et al., 1994; Habtezion et al., 2005). Furthermore, mice with K8 deletion that have been treated with carcinogens or have a tumor suppressor mutation, are more sensitive to develop tumors compared to mice with K8 (Misiorek et al., 2016; Stenvall et al., 2021).

In absence of oxygen and/or under the influence of growth factors, the hypoxia signaling is activated. In general, the activation of the pathway is correlated

with pathological conditions such as numerous heart conditions and tumor growth, however, in some instances it can also be a result of non-pathological conditions such as in high intensity training (Lundby, Gassmann & Pilegaard, 2006; Lee et al., 2019). The activated pathway increases the translation and stabilization of the well-known transcription factor HIF-1α. Once stabilized, HIF-1α binds and dimerizes with its partner aryl hydrocarbon receptor nuclear translocator (ARNT) and binds to its cofactors p300 and CREB- binding protein (CBP), after which the complex can activate the transcription of over 100 genes. The proteins resulting from the transcriptional activation work together to e.g., regulate the metabolism to avoid oxidative damage, increase angiogenesis to the hypoxic area and increase the amount of erythrocytes for a higher oxygen flow (Semenza, 2007).

Previous experiments in our laboratory indicate that K8 is involved in regulating the hypoxia pathway in the colon. The aim of this thesis was to develop a deeper understanding of the cross play between K8 and the hypoxia pathway, and to investigate what outcome K8 loss has in regard to the signaling in the colonic epithelial cells.

2 LITERATURE OVERVIEW

2.1 THE LARGE INTESTINE

2.1.1 Function and macroanatomy

The large intestine is 1.5 meters long and is the last part of the gastrointestinal tract. It is divided into cecum, appendix, colon (ascending, transverse, descending and sigmoid), rectum and lastly the anal canal together with the anus (**Figure 1**.). The main function of the large intestine is to finalize the digestion of nutrients, and absorb water, electrolytes, and vitamins (Nigam, Knight & Williams, 2019).

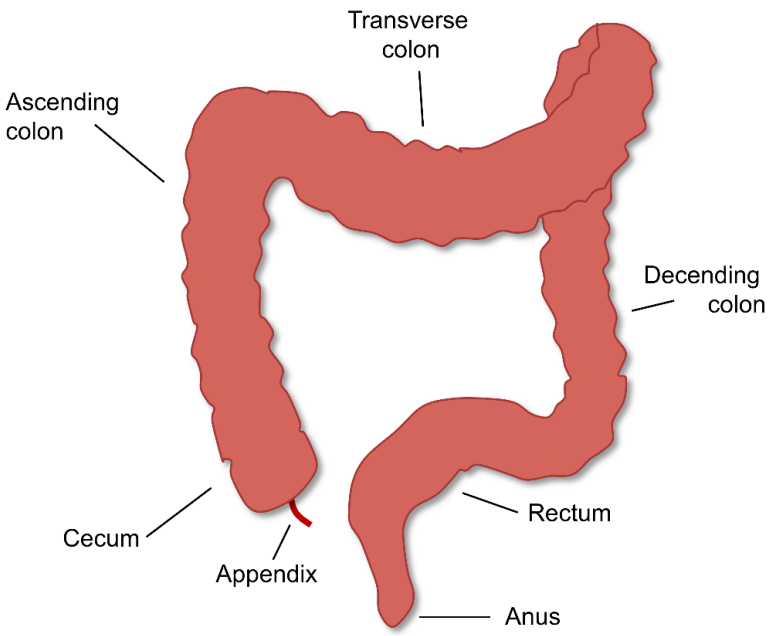

Figure 1. Illustrating the macroanatomy of the colon. Food residues reach the large intestine in the cecum. From cecum it travels to the colon (ascending, transverse, and descending colon), after which it passes the rectum and is discarded from the body through the anus.

Most of the nutrients and water is absorbed in the stomach and small intestine so food residues reaching the large intestine are in general low on products for digestion and absorption, but the large intestine still poses a big role in regulating the body homeostasis (Szmulowicz, Hull, 2011; Azzouz, Sharma, 2018). The process in the large intestine starts with food residues reaching the cecum (first part of the large intestine), which triggers muscular movements pushing the residues back and forth for processing. In the colonic epithelial cells, sodium ions are pumped out through the basolateral side via Na^+/K^+ ATPase pumps creating an electrochemical gradient that leads to sodium ions from the food residues in the colon to be absorbed on the apical side. This in turn leads to an osmotic gradient causing water to be absorbed from the lumen. Sodium is by far the most important absorbed electrolyte; however, chloride is also absorbed by similar mechanisms (Szmulowicz, Hull, 2011). Notably, a change in the osmotic balance can cause a decrease in water absorption, leading to diarrhea.

The large intestine is one of the most densely populated ecosystems of the world with millions of bacteria growing there (Garrett, Gordon & Glimcher, 2010). Since it does not have any own enzyme production or secretion, the bacteria play a vital role in the processing of the residual nutrients. The processing occurs via fermentation, where carbohydrates and proteins are digested into smaller compounds, which are used to fuel the host's metabolism (Cummings, Englyst, 1987; Macfarlane, Macfarlane, 2011). In addition to processing nutrients the bacteria also participate in the production of vitamins K, B, and biotin via fermentation, which is important especially when the dietary consumption of these vitamins is low (Azzouz, Sharma, 2018). Furthermore, the bacteria work as a first line of defense against pathogenic bacteria, by competing for the microenvironment (Macfarlane, Macfarlane, 2012).

2.1.2 Colon structure and microanatomy

The colon consists of four tissue layers, the mucosa, which is the innermost layer, the submucosa, the muscularis externa and lastly the serosa (**Figure 2.**).

The mucosa is further divided into epithelium, lamina propria, and muscularis mucosa. The single-cell layered epithelium consists of crypts covered with a number of different epithelial cell types, which will be discussed in more detail below. Lamina propria is the connective tissue layer found beneath the epithelium. It contains nerves, blood vessels, lymph vessels and various cells, such as fibroblasts and white blood cells. All of these components work together to supply the epithelium with support, oxygen, nutrients and a second line of defense against possible pathogens that have breached the surface (Mescher, 2013; Caballero, Finglas & Toldrá, 2015). Muscularis mucosa is composed of smooth muscle cells stretching both longitudinally and circularly around the lamina propria, assisting the peristaltic moments of the colon.

The submucosa is in direct contact with muscularis mucosa and consists of connective tissue. It consists of the same cells as the lamina propria and works as a passageway for the nerves, blood vessels and lymph vessels to the lamina propria.

Outside the submucosa lies a second layer of smooth muscle cells called the muscularis externa. Similarly to the muscularis mucosa, it consists of both longitudinal and circular muscle cells, however a significantly thicker layer, and contributes to most of the peristaltic movements. Lastly, the serosa, made of connective tissue and mesothelial cells, wraps the whole structure (Bustos-Fernández, 2013; Caballero, Finglas & Toldrá, 2015).

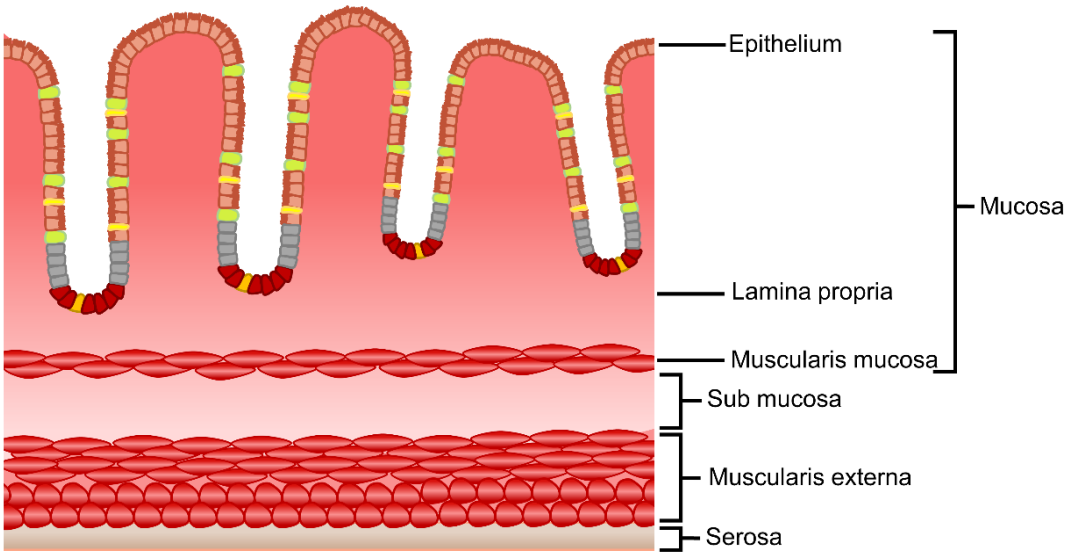

Figure 2. The layers of the colon. A theoretical cross section of colon tissue. The innermost layer, mucosa, is divided into epithelium, lamina propria and muscularis interna. The mucosa is followed by sub mucosa, muscularis externa and serosa, which is the outermost layer.

As previously mentioned, the epithelium creates invaginations called crypts on the inner surface of the colon. The crypts consist of stem cells, transit amplifying cells, absorptive enterocytes, mucus-producing goblet cells, signal transducing enteroendocrine cells and a low number of antimicrobial peptide secreting Paneth cells (from the cecum to the transverse colon) (Caballero, Finglas & Toldrá, 2015). Due to the stem cells located in the bottom of the crypts, the epithelium undergoes rapid renewal. The process of renewal and differentiation begins with the stem cells dividing into new stem cells and transit amplifying cells that are regulated by a number of signaling pathways such as Notch, Wnt and bone morphogenetic protein signaling (BMP) (Humphries, Wright, 2008; Polari et al., 2020). The cells start to differentiate and push up along the crypt walls, after which they go into a non-replicative state, i.e., when they are fully differentiated into the cells mentioned above. From there they move towards the lumen of the colon where they eventually die from apoptosis, and they detach into the lumen (**Figure 3.**).

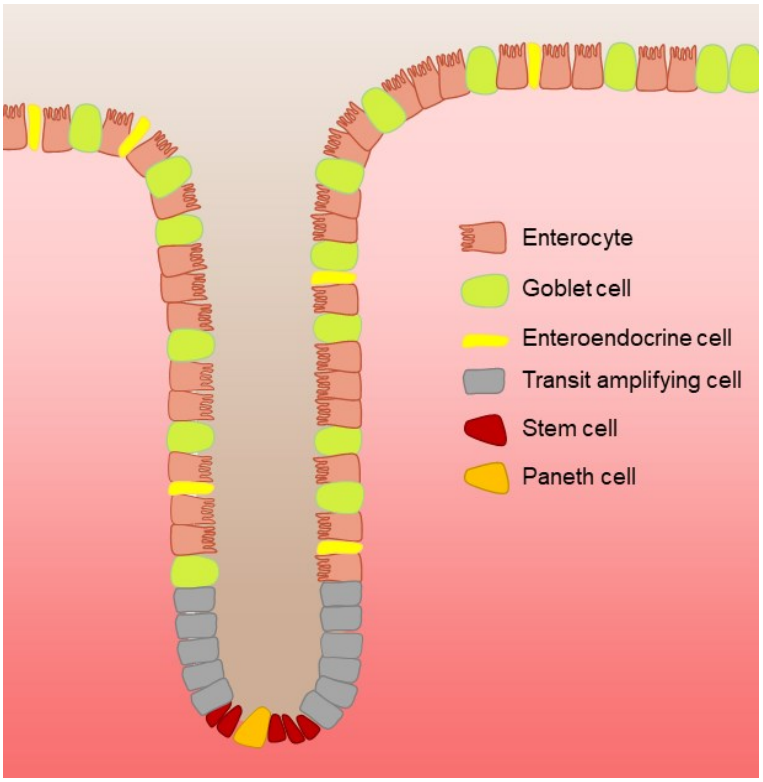

Figure 3. The structure of a colonic crypt. The figure illustrates the theoretical composition of a colon crypt. In the base of the crypt the stem cells divide into transit amplifying cells, which differentiate to become enterocytes, goblet cells, enteroendocrine cells and Paneth cells (small number from the cecum to the transverse colon).

Alongside the bacterial ecosystem, the epithelium participates in the first line defense against pathogens. Because of its mucus and antimicrobial peptide production together with the tight junctions between the epithelial cells it creates a nearly impregnable defense wall (Garrett, Gordon & Glimcher, 2010).

2.2 INTERMEDIATE FILAMENTS

Composed of dynamic polymer building blocks, the cytoskeleton aids the cells in movement, molecule trafficking, organization and gives them structural support and stiffness. The cytoskeleton is divided into three groups,

microfilaments, microtubules and intermediate filaments (Fletcher, Mullins, 2010).

Microfilaments, also known as actin filaments, are built from a large number of actin molecules attaching to each other, thus, creating a polarized filament. Actin filaments are thin and flexible; however, they cross-link to each other to create a rigid three-dimensional network (Cooper, Hausman & Hausman, 2007; Fletcher, Mullins, 2010). Besides giving support to the cell, actin filaments are e.g., strongly involved in movement and migration of the cell via protrusion, and they are also one of the main components in sarcomeres, giving us the ability to contract muscles (Heck et al., 2020).

Microtubules are the stiffest and most dynamic of the filaments. They are built from repeating α- and β-heterodimers, creating a polarized hollow tubule structure. Because of their high dynamics and polarization, they are the main passageway for intracellular trafficking via a range of motor proteins “walking” on them. Furthermore, microtubules create the mitotic spindle during cell division that separates the chromosomes, thus, they possess a non-replaceable function in cells (Nogales, 2001; Fletcher, Mullins, 2010).

There are at least 73 genes encoding for intermediate filament proteins (Omary, 2009). The intermediate filaments are flexible and relatively insoluble proteins that cross-link to other cytoskeletons to create structural support and help cells to manage mechanical stress (Fletcher, Mullins, 2010). Contrary to actin filaments and microtubules, they are not polarized, meaning they are not part of intracellular trafficking; they have a cell and tissue specific expression, and their dynamics are more spontaneous and regulated mostly by phosphorylation (Omary, Coulombe & McLean, 2004; Leube, Schwarz, 2016).

The intermediate filaments are divided into six categories based on their diversity in size and amino acid sequence (Table 1.). Type I and II IFs include acidic keratins (Type I) and basic/neutral keratins (Type II) and are located in

epithelial cells, as well as in hair and nails. The keratins in epithelia play a vital role in structurally supporting cells, attaching cells to one another, and providing them with protection for chemical and mechanical stresses (Jacob et al., 2018).

Type III IFs desmin and syncoilin are located in muscle cells at the sarcolemma and the sarcomeres, where they provide support and transduce mechanochemical signaling (Poon et al., 2002; Viedma-Poyatos, Pajares & Pérez-Sala, 2020). Vimentin is found in mesenchymal cells and to some extent also in astrocytes, where it has the main role of anchoring organelles and providing support (Katsumoto, Mitsushima & Kurimura, 1990). Since it is located in mesenchymal cells, it has been used as a diagnostic marker for epithelial to mesenchymal transition in cancer research (Liu et al., 2015). GFAP is a protein mainly located in astrocytes where it participates in e.g., migration and damage response in inflammation and trauma (Viedma-Poyatos, Pajares & Pérez-Sala, 2020). Last in the group is peripherin, which is expressed in peripheral neurons. It is the least studied Type III filament; however, studies suggest that it plays a role in regeneration of damaged neurons and axonal elongation during development (Escurat et al., 1990; Troy et al., 1990).

Type IV IF synemin is also located mainly in muscle cells. Studies show that it supports the sarcolemma and binds to α-actinin in the sarcomeres, where it cross-links to other IFs (Russell, 2020). α-internexin and neurofilaments are located mainly in the central nervous sytem, however, also to some extent in the peripheral nervous system. α-internexin is expressed during development, and its expression decreases during maturation when neurofilaments start to outnumber in mass. Their role is to provide structural support to the thin and long neurons (Cooper, Hausman & Hausman, 2007; Zhao, Liem, 2016). Some studies suggest that Type IV α-internexin and Type III peripherin are part of the Type IV neurofilaments; however, this has not been established. Last in the group of Type IV IFs is nestin. It is located in the neuroepithelium and to some extent in neural stem cells. As with many other IFs it has the role of organizing structures; however, studies suggest it has a role in regulating the

dynamics of other IFs, microfilaments and microtubules (Michalczyk, Ziman, 2005).

Type V IFs are composed of lamins A/C, B1 and B2, and are found in the nuclear lamina; thus, they are not part of the cytoplasmic cytoskeleton. They are not expressed tissue specifically like other IFs, meaning they can be found in all cells with a nucleus. Their main function is to provide support and shape to the nucleus; however, they also participate in disassembling the nuclear envelope during mitosis (Gruenbaum, Foisner, 2015).

The last category, Type VI, includes phakinin and filensin, which are located in fiber cells in the lens. Cataract, i.e., cloudy eyes, has been correlated with mutated phakinin and filensin, which suggests that they play a role in the opacity of the fiber cells (Shiels, Hejtmancik, 2015).

Table 1. The types of intermediate filaments. Table inspired by (Coulombe, Wong, 2004; Omary, 2009).

Protein	IF Type	Localization
Acidic Keratins	I	Epithelium, hair, nails
Basic Keratins	II	Epithelium, hair, nails
Desmin, Syncolin	III	Muscle cells
Vimentin	III	Mesenchymal cells
GFAP	III	Astrocytes
Peripherin	III	Peripheral neurons
Synemin	IV	Muscle cells
α-Internexin, Neurofilaments	IV	Central nervous system
Nestrin	IV	Neuroepithelium
Lamin A/C, B1, B2	V	Nuclear lamina
Phakinin, Filensin	VI	Fiber cells (Lens)

2.2.1 Assembly of intermediate filaments

As previously described, both microfilament and microtubule elongate by addition of small polymers to create a polarized structure. This is not the case for intermediate filaments as they elongate via addition of bigger subunits (compared to MF and MT) to either end of the growing filament, and interestingly also along the length of the filament (Leube, Schwarz, 2016).

The assembly of intermediate filaments starts when two protein monomers bind parallelly to each other to create a so-called coiled-coil dimer. The dimers then bind anti-parallelly to a second pair of dimers, creating a tetramer, which results in loss of polarity. In general, 8 tetramers assemble laterally into a ULF and the ULFs combine longitudinally to create the final structure of the intermediate filaments (**Figure 4.**) (Herrmann et al., 2007).

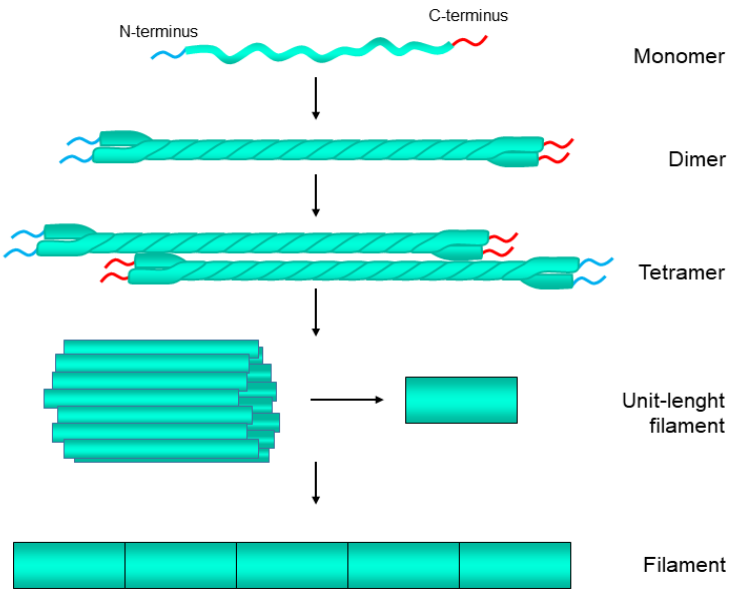

Figure 4. The assembling of an intermediate filament. The assembly starts by two monomers coiling around each other (N-terminus to N-terminus) creating a coiled-coil dimer. The dimers interact with each other in an anti-parallel fashion (N-terminus to C-terminus) to create a non-polarized tetramer. Approximately 8 tetramers assemble to create unit-length filaments, which bind end-to-end to create the final intermediate filament.

Depending on the type/category of the intermediate filament they can assemble in different manners. Some filaments, such as keratins, always form Type I and Type II heterodimers. Others like vimentin and desmin can form homodimers as well as heterodimers (Herrmann et al., 2007).

2.2.2 Keratins

The keratin family consists of 54 genes coding for Type I (K9-K28 and K31-K40) and Type II (K1-K8, K71-K86) filaments that interact with each other to create heterodimers. Keratins are expressed in a highly tissue-specific manner and are located in simple epithelia such as the intestine, pancreas and lungs, and stratified epithelia in the skin, as well as in hair and nails (Polari et al., 2020).

The primary structure of keratins differs from each other, leading to differences in size, charge, and polarity. Interestingly, however, conservational studies show considerable similarity between particular keratins from different species, further suggesting they have a vital role in the cell (Fuchs, 1983). Even though the primary structure is incompatible between different keratins, they generally have a similar secondary structure with the same domains. The structures consist of a head domain (N-terminal), a-helical rod domain and a tail domain (C-terminal) (Bragulla, Homberger, 2009) (**Figure 5.**).

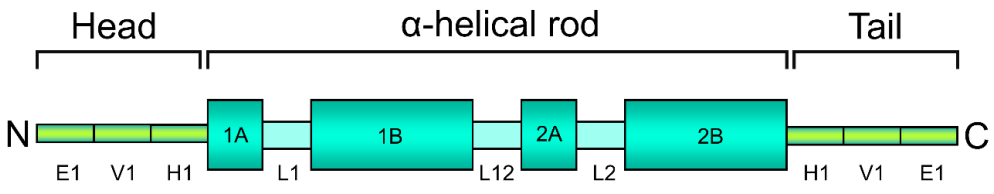

Figure 5. The secondary structure of keratins. Figure 5 illustrates the secondary structure of keratins with the N-terminal head domain, followed by the rod domain and lastly the C-terminal tail domain. The figure also illustrates the subdomains. Inspired by Bragulla, Homberger, 2009.

Keratin filaments are dynamic and flexible proteins that can resist high tensile strength. Upon stimulation, they can adapt to their environment via a range of post-translational modifications, such as phosphorylation and ubiquitination, and interactions with some adaptor proteins, such as 14-3-3 (Jacob et al., 2018).

The most notable and understood function of the keratins is their role in stress and damage protection. Studies show that keratins are upregulated and hyperphosphorylated during stress, indicating that keratins work for fortification/reinforcement and structural remodeling (Toivola et al., 2005; Omary et al., 2006; Snider, Omary, 2014). Keratins bind to other cytoskeletal filaments, to the nucleus, cell-cell (desmosomes) and cell-matrix (hemidesmosome) junctions, which adds structural rigidity and resistance against mechanical stress (Moll, Divo & Langbein, 2008). Compared to microfilaments and microtubules, keratins have been shown to manage greater amounts of mechanical stress, further demonstrating their importance in the protection of cells (Jacob et al., 2018).

Beyond their function in stress protection, keratins are also known regulators of various signaling pathways (Pallari, Eriksson, 2006). They regulate cell survival and death through pro-apoptotic and pro-survival components, such as tumor necrosis factor receptor 2 (TNFR2) and focal-adhesion kinase-1 (FAK). Moreover, they influence the cell mobility and migration patterns of cells by regulating the signaling molecules Src kinase (Src) and receptor for activated protein kinase C (RACK1). Finally, studies show that keratins are involved in regulating cell growth and proliferation by interacting with signaling molecules such as protein kinase B (Akt) and protein kinase C (PKC). All these key components are subjected to both positive and negative regulation by keratins. As an example, studies show that Akt activity is increased by K14 and K17, whilst it is suppressed by K8/K18 and K10 (Pan, Hobbs & Coulombe, 2013). Taken together, this demonstrates the complexity by which keratins influence cellular processes through signaling.

2.2.3 Keratins in the colon

The keratins in the colon are located in the mucosa's inner layer called the epithelium, where they provide structural support and protect cells from stress. The most dominant keratins in the colon are K8, K18, K19 and K20; however, studies also suggest that there are lower concentrations of K15, K23, K24 and K80 to be found. Furthermore, in contrast to a healthy human colon, the mice colon also expresses lower concentrations of K7 (Polari et al., 2020).

K8, K18, K19, K80, K23 and K24 are evenly distributed in the epithelium from the bottom of the crypts to the lumen. In contrast, K15 is located at the bottom of the crypts, and K20 is found in more differentiated cells and more highly expressed in upper parts of the crypt (**Figure 6.**) (Polari et al., 2020).

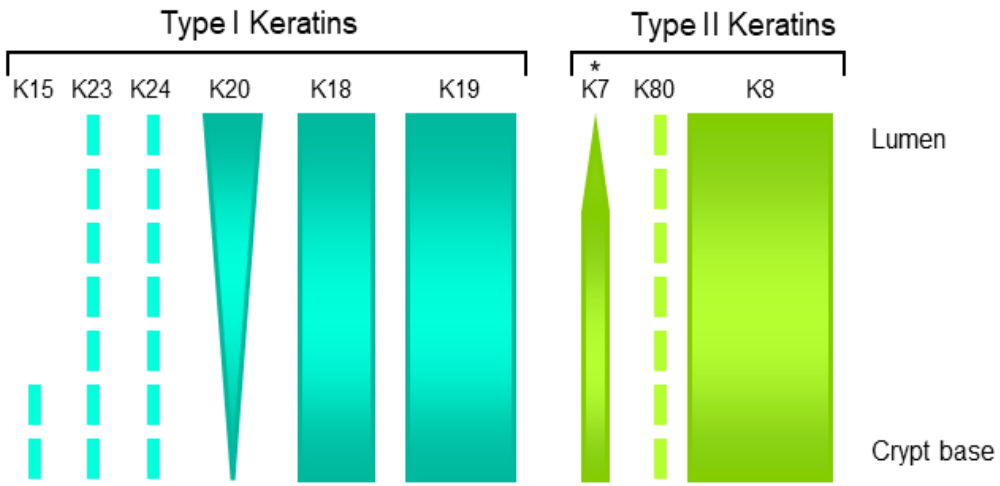

Figure 6. Distribution of keratins in the colon. Type I and Type II Keratin distribution in the colon epithelium. On the upper side is the colon lumen and at the bottom is the base of the crypts. Dotted lines represent a low expression/less studied keratins and bars represent a higher expression rate (with thicker bars having higher expression). *= expressed in mouse colon, but not in human. The illustration is inspired by Polari et al., 2020.

2.2.4 Colon disorders linked to K8

Keratins in general are involved in as much as 60 keratinopathies, i.e., disorders caused by keratin mutations. The diseases are mostly related to the skin and liver, however, keratinopathies can also be found in the eyes, hair, and colon (Omary, 2009; Toivola et al., 2015).

The clear role of keratins in colon disorders is still a mystery. The first evidence of the role of K8 in colon homeostasis was shown in a study where it was discovered that $K8^{-/-}$ mice developed epithelial hyperplasia, followed by colitis, rectal prolapse and diarrhea, which resembles a form of human inflammatory bowel disease (IBD) (Baribault et al., 1994). The mice have been shown to suffer from T-helper 2 (Th2) colitis, with increased CD4+ infiltration in the lamina propria, increased Th2 cytokine production and expression of major histocompatibility complex 2 (MHCII) antigens on the epithelial cells (Habtezion et al., 2005). Furthermore, microarray analysis of the colonic epithelial crypts showed that $K8^{-/-}$ mice had altered apoptotic pathways, causing them to be more resistant to apoptosis compared to $K8^{+/+}$ mice, which could to some extent explain the hyperproliferative phenotype (Habtezion et al., 2005). Interestingly, in both of Habtezions studies when knockout mice were treated with antibiotics, both the inflammation and apoptotic resistance were regressed and normalized, suggesting that the microbiota has a central role in a defective colon. Moreover, studies show an altered Na^+ and Cl^- transport leading to a change in water balance and eventually the previously noted diarrhea (Toivola et al., 2004).

Colorectal cancer is one of the most common cancers in the world. Hyperplasia, inflammation, and resistance to apoptosis as noted in $K8^{-/-}$ mice are all hallmarks of cancer, however, $K8^{-/-}$ mice do not develop spontaneous tumors as one might expect. Nevertheless, $K8^{-/-}$ mice subjected to carcinogens or with a mutation in the tumor suppressor gene Apc developed colorectal tumors, whilst $K8^{+/+}$ mice under the same conditions did not. The tumor development observed in the experiments is connected with an upregulation of IL-22 and downregulation of IL-22BP, its repressor (Misiorek

et al., 2016). This leads to an activated JAK/STAT signaling that, in turn, stimulates cells into proliferation and tumorigenesis (Kirchberger et al., 2013). Recent studies by Stenvall et al. (2021) further confirmed the role of K8 in protecting the colon from tumorigenesis, by showing that deletion of K8 in colonic epithelial results in disrupted tissue integrity, increased proliferation, and increased sensitivity to the carcinogen azoxymethane (AOM) in the colon. All in all, the results suggest that keratins, specifically K8, have a vital role in protecting the colon from tumor development.

2.3 THE HYPOXIA PATHWAY

In the absence of oxygen (hypoxia) in cells, the hypoxia pathway is activated. Once the pathway is activated, it results in the stabilization of the transcription factor HIF-1α, which in turn activates the transcription of hundreds of proteins that regulate cell metabolism, proliferation, angiogenesis, erythropoiesis, and cell death. The accumulative effect of these processes is meant to protect the cells and tissue from stress damage and to increase the flow of oxygen to the affected area (Semenza, 2007; Li et al., 2019).

The activated pathway is generally correlated with pathology but is also connected to normal physiology, such as in the stem cell niche where it aids in keeping stem cells undifferentiated, or in the skeletal muscle where it regulates adaptive responses during high intense training (Lundby, Gassmann & Pilegaard, 2006; Mohyeldin, Garzón-Muvdi & Quiñones-Hinojosa, 2010; Lee et al., 2019). The most notorious culprit in hypoxia-related pathology is cancer. Scientists have found a causal interference between the pathway and cancer, where it enforces e.g., angiogenesis, proliferation, and metastasis, driving tumorigenesis forward (Masoud, Li, 2015). The pathway is regulated in two major ways: transcriptional regulation and the regulation of HIF-1α stability.

2.3.1 Regulation of HIF-1α stability and activation

In normoxic (normal oxygen level) conditions, HIF-1α is continuously degraded by the oxygen-dependent proteins prolyl hydroxylase domain-2 (PHD2) and arrest-defect-1 (ARD-1). PHD2 hydroxylates HIF-1α on two proline residues (P402 and P565) and ARD-1, which is an acetyl transferase enzyme, acetylates HIF-1α on lysine 532 (K532) (Deep, Panigrahi, 2015; Masoud, Li, 2015). Acetylation does not require oxygen, meaning that ARD-1 is not theoretically dependent on oxygen, however, studies show that its activity decreases in pace with decreased oxygen (Jeong et al., 2002). These three marked residues will be detected by the subunit of the E3 ubiquitin ligase, von Hippel-Lindau (VHL), which tags HIF-1α with polyubiquitin (**Figure 7.A**). The ubiquitin tags are recognized by proteasomes, leading to the degradation of HIF-1α (Semenza, 2007).

Mouse double minute 2 (MDM2) and p53 are also part of regulating the stability of HIF-1α, however, they are not dependent on oxygen. p53 binds to HIF-1α, which is recognized by ubiquitin ligase MDM2 that marks HIF-1α with ubiquitin for its degradation by proteasomes (**Figure 7.B**) (Deep, Panigrahi, 2015). Studies have also shown that besides interacting directly with HIF-1α, p53 can also interfere with HIF-1α binding to DNA. Although unclear, it is believed that p53 is also similarly active during hypoxia, however in instances like cancer, p53 is usually mutated leading to higher levels of HIF-1α (Sermeus, Michiels, 2011).

Unlike the previously mentioned protein, factor inhibiting HIF-1 (FIH-1) does not participate in the regulation of HIF-1α stability, but its activation. FIH-1 hydroxylates asparagine 803 (Asn803), which interrupts the binding of HIF-1α cofactors p300 and CBP and thereby inactivates the transcriptional activity of HIF-1α (**Figure 7.C**) (Semenza, 2007).

In the absence of oxygen, PHD2, ARD-1 and FIH-1 cannot hydroxylate and acetylate their target, HIF-1α. This results in a stable HIF-1α, which translocates to the nucleus where it interacts with its sub-unit ARNT and co-

activators p300 and CBP. In the nucleus, the complex binds to the hypoxia response element domain of DNA and activates the transcription of their target genes such as vascular endothelial growth factor (VEGF), B-cell lymphoma 2 (Bcl2) and claudin-1 (Harris, 2002; Chee, Lohse & Brothers, 2019).

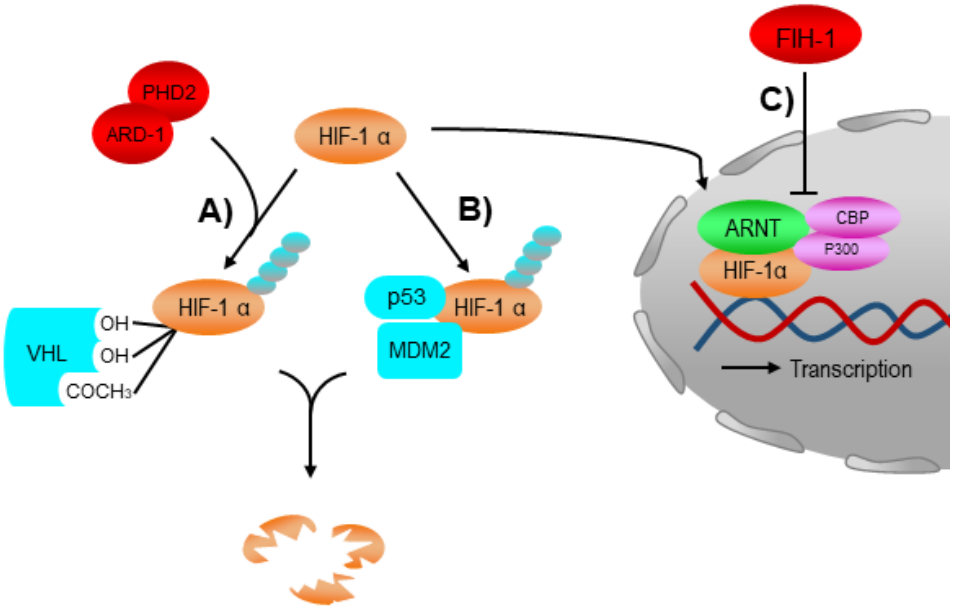

Figure 7. The regulation of HIF-1α stability. The figure illustrates the pathways regulating HIF-1α stability and activation. **(A)** PHD2 hydroxylates two proline residues and ARD-1 acetylates a lysine residue on HIF-1α. These modifications are recognized by VHL, which leads to ubiquitination followed by degradation of HIF-1α. **(B)** p53 bound to HIF-1α is recognized by MDM2. This leads to ubiquitination and proteasomal degradation of HIF-1α. **(C)** FIH-1 hydroxylates HIF-1α, which decreases its binding to cofactors, p300 and CBP, needed for transcriptional activation.

2.3.2 Transcriptional regulation

During normoxia RTKs activated by growth factors can influence the hypoxia pathway. Even though HIF-1α is actively degraded, the PI3K/Akt/mTOR pathway and the RAS/RAF/MEK/ERK/MNK pathway can to some degree counter the effect of proteasome degradation by enhancing HIF-1α mRNA

translation, thus, increasing the transcriptional activity of HIF-1α (**Figure 8.**) (Ziello, Jovin & Huang, 2007).

The PI3K/Akt/mTOR pathway starts with the activation of a receptor tyrosine kinase (RTK). The RTK activates phosphoinositide 3-kinase (PI3K), which in turn activates Akt, and finally Akt activates mammalian target of rapamycin (mTOR) (here mTORC1). mTOR will then go on to phosphorylate S6 kinase (S6K) and 4E- binding protein 1 (4E-BP1). Phosphorylation of S6K results in the kinase activating S6, which enhances translation, whilst the phosphorylation of 4E-BP1 results in a complex dissociation between it and its partner eukaryotic translation initiation factor 4E (eIF-4E), which further enhances translation of HIF-1α (Masoud, Li, 2015).

The RAS/RAF/MEK/ERK/MNK pathway is also activated by RTKs leading to a similar cascade where each component activates the next. Extracellular signal-regulated kinase (ERK) will also phosphorylate S6K and 4E-BP1, and in addition it will also phosphorylate HIF-1α coactivators p300 and CBP, increasing the transcriptional activity of HIF-1α. Furthermore, MAP kinase-interacting kinase (MNK) will phosphorylate eIF-4E, which increases its effectiveness in HIF-1α translation (Masoud, Li, 2015).

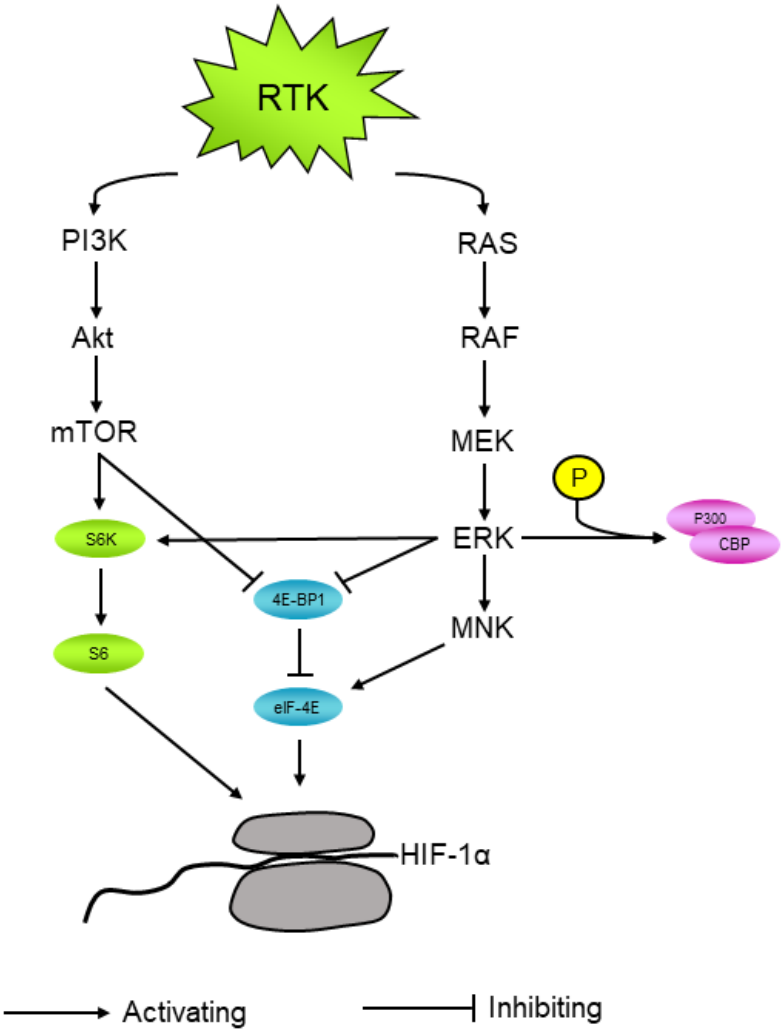

Figure 8. Activated RTK regulates transcription of HIF-1α. Two of the biggest survival pathways are activated upon stimulations via RTK. This leads to a signaling cascade, which ends with mTOR and ERK inactivating 4E-BP1 and activating S6K. ERK also phosphorylates HIF-1α co-factors p300 and CBP and MNK activates eIF-4E. All of the mentioned events lead to increased HIF-1α translation.

2.3.3 Hypoxia signaling in the intestine

The intestine has a significantly lower oxygen tension than most of our organs, which is partly explained by the activity of the complex microbiota and the metabolism of the colon epithelium (Kelly et al., 2015). The hypoxia signaling

and the general oxygen dynamics have a central role in maintaining intestinal homeostasis, and the disruption of this homeostasis has been shown to be involved in the disease development of IBD and colorectal cancer (Singhal, Shah, 2020).

HIF-1α has been shown to have an important role in maintaining the pathogen protecting mucosal barrier of the intestines. It regulates the transcription of several mucins needed for mucus, as well as regulate the antimicrobial peptide β-Defensin-1 production (Singhal, Shah, 2020). Furthermore, it regulates the transcription of claudin-1, which is a protein found in the tight junctions in the intestine and important for intestinal barrier integrity. Cell model studies have shown that knocking out HIF-1α results in problems with tight barrier formation, which can be completely reversed by the expression of claudin-1, thereby demonstrating the importance of HIF-1α in the intestines (Saeedi et al., 2015).

Moreover, the hypoxia signaling influences the intestinal barrier indirectly to assist with repairing damage to the gut epithelia. This process is driven by hypoxia signaling-mediated regulation of the ATP and adenosine pool. In detail, HIF-1α induces transcription of CD39, CD73, whilst HIF-1α isoform, HIF-2α, regulates the transcription of components in the creatine/creatine kinase pathway (Singhal, Shah, 2020). CD39 and CD73 are membrane-bound proteins in charge of degrading ATP to adenosine, which is an important wound healing signaling factor (Synnestvedt et al., 2002; Aherne et al., 2015). The creatine/creatine kinase pathway in turn is crucial for the production and maintenance of a high energy ATP pool, which is necessary for a proper wound repair (Glover et al., 2013). In addition to regulating the ATP/adenosine pool, HIF-1α regulates the peptide Trefoil factor-3 expression, which enhances the epithelial barrier via regulating the function of tight junctions and assists the gut in regeneration and repair after damage (Aihara, Engevik & Montrose, 2016; Singhal, Shah, 2020).

3 HYPOTHESIS AND AIMS

3.1 HYPOTHESIS

My hypothesis is that K8 influences the hypoxia pathway by interactions with the PI3K/Akt/mTOR pathway and K8 deletion leads to higher levels and increased nuclear translocation of HIF-1α. Furthermore, I hypothesize that subjecting colorectal cancer cells to hypoxia will increase their keratin expression.

3.2 AIMS

Previous unpublished work in our laboratory have indicated that K8 deletion results in a more hypoxic colon and an altered hypoxia pathway (**Supplemental figure 1.**). Thus, the aim of this study is to further investigate the possible connection between K8 and the hypoxia signaling and try to answer questions about what K8 loss results in, with regard to the hypoxia pathway and where the possible interplay may be.

3.2.1 The specific aims

1) Determine if K8 loss leads to an altered hypoxia signaling *in vivo* and determine if the outcome is replicable *in vitro* and *ex vivo*.

2) Determine how K8 is shifting the hypoxia pathway activation.

3) Determine if there is a complex formation between K8/K18 and the transcription factor HIF-1α.

4) Determine if K8 loss leads to altered nuclear translocation of HIF-1α.

5) Determine if keratins are upregulated *in vitro* as a response to hypoxic stress.

4 MATERIALS AND METHODS

4.1 MOUSE MODELS AND ETHICS

In this thesis $K8^{+/+}$, $K8^{-/-}$, $K8^{Flox/Flox}$ and $K8^{Flox/Flox}$;Villin-Cre mice were used. The K8 full knockout, $K8^{-/-}$, mice (FVB/N background) have a segment deleted from the Krt8 gene, which leads to them not expressing K8 in the entire mouse. In contrast, K8 conditional knockout mice, $K8^{Flox/Flox}$;Villin-Cre (C57BL/6 background), have a K8 deletion in villin expressing cells. The mice have an inserted villin promotor in the gene for the Cre enzyme, which leads to Cre being expressed only in cells expressing villin. When expressed, Cre goes on to cut the LoxP sequences inserted in the Krt8 gene, thus, depleting K8 from the epithelium (Stenvall et al. 2021).

The genotypes of the mice were confirmed by PCR of earpieces and western blot analysis. The mice were kept in the animal facility of University of Turku and were experimented on with the license ID: ESAVI/16359/2019 that was granted by the National Animal Ethics Committee of Finland.

4.2 CELL CULTURING AND ORGANOID ISOLATION

4.2.1 Cell culturing

The cells used in this thesis were colorectal cancer cells Caco-2 cells and single cell clones of genetically modified Caco-2-K8 CRISPR/Cas9 wild type ($K8^{+/+}$) and Caco-2-K8 CRISPR/Cas9 Knockout ($K8^{-/-}$) cells. The cells were grown on 10 cm dishes and were split at ~ 80% confluency. The splitting started with removing the old media, washing them 2 times with 1 x phosphate buffered saline (PBS) (Biowest, MO, USA) and adding 1 ml of trypsin (Biowest). Trypsin is a serine protease and works by cleaving the peptides holding the cells to the dish, allowing them to be suspended. The cells were placed back into the incubator for 5 minutes, whereafter ~ 8 ml of media was added to the dish and the cells were collected in a Falcon tube which was

centrifuged for 4 minutes at 1000 x g. The media was discarded (not disturbing the pellet) and the pellet was resuspended in 8 ml of media. The desired number of cells (see next section) were placed in a new dish and was topped off with medium to a total volume of 10 ml.

$K8^{+/+}$ CRISPR/Cas9 cells and Caco-2 cells were split 1:4 and $K8^{-/-}$ CRISPR/Cas9 was split 1:3 because of a slower growth rate. The medium used was Dulbecco's Modified Eagle's Medium - high glucose (Sigma-Aldrich, MO, USA) containing 10% FPS serum (20% for the CRISPR/Cas9 cells), 2 mM L-Glutamine and 100 µM antibiotics (P/S). Cells grew at 37 °C and 5% CO2.

4.2.2 Organoid isolation and culturing

A mouse was sacrificed with CO_2 and its large intestine was removed and placed on a glass plate (on ice). Abdominal adipose tissue was removed, and the intestine was cut open and washed with 1 x PBS. After this, a 50 ml Falcon tube was filled with 15 ml of cold 1 x PBS and the colon was cut into approximately 2 mm segments which were placed in the Falcon tube. The tube was vortexed for 5 seconds and then the PBS solution was poured off using a tea strainer. Three previous steps (vortexing, pouring PBS away and adding new PBS) were repeated 15-20 times. After the last PBS wash, 30 ml of 5 mM RT ethylenediaminetetraacetic acid (EDTA) (pH 8.0) (diluted in PBS) was added to the intestinal pieces, and the tube was incubated at room temperature (RT) on rotation for 20 minutes.

After the incubation, everything was moved to the laminar cabinet where the EDTA solution (on ice) was poured out, 10 ml of cold 1 x PBS was added, and the tube was inverted a few times to rinse off the EDTA. The PBS was then poured out and the intestinal segments were placed in a new Falcon tube with 10 ml of cold 1 x PBS. The tube was shaken vigorously 5 times to loosen the crypts and the PBS solution was placed in a new 50 ml Falcon tube marked as fraction 1. The previous three steps were repeated until there were 8

fractions. After that, 10 µl of each fraction was pipetted onto a slide to be analyzed under a microscope to examine the number of crypts. The 4 fractions with the most intact crypts and least debris were merged into the same Falcon tube and filled to a total volume of 50 ml with DMEM/F-12 (STEMCELL, Vancouver, Canada). The tube was centrifuged 300 x g, 5 minutes at 4 °C. The supernatant was then poured off and the crypt pellet was dissolved in 1 ml of cold DMEM/F12.

The number of crypts in the DMEM/F-12 solution was then counted and a new solution was mixed of DMEM/F12 and Matrigel in a 1:1 ratio, diluted so that there were 100 crypts per 50 µl solution. In the next step 50µl of the solution was applied to flame sterilized coverslips in a 24-well plate. The plate was then placed in the incubator (37°C, 5% CO_2) for 10 minutes. Meanwhile, Intesticult Growth Medium (STEMCELL) and ROCK inhibitor (Adooq Bioscience, CA, USA) was added to a final concentration of 10 µM and P/S (penicillin-streptomycin) to a final percentage of 0.5%, after which 500 µl of the medium was added to each well. The organoids were cultured in 37 °C, 5% CO_2 and their medium (Intesticult Growth Medium and 0.5% P/S, but no ROCK inhibitor) were changed 3 times a week.

4.2.3 Hypoxia induction

This thesis used two methods to induce hypoxia or activate the hypoxia pathway chemically. The first method was to use a hypoxia chamber (InvivO2 400, Ruskinn Technology (now Baker), Bridgend, Great Britain) with controlled oxygen concentration. In this thesis, cells were treated in the chamber 4 hours and organoids 16 hours at 37 °C and 1% oxygen, and the control samples grown in an incubator at 37 °C and 5% CO_2. This is considered the most reliable method for studying hypoxia as it resembles the physiological condition of *in vivo* hypoxia. The second method was to use the compounds cobalt chloride ($CoCl_2$) (Sigma-Aldrich) and dimethyloxalylglycine (DMOG) (Cayman chemicals, MI, USA), which work by inhibiting part of the HIF-1α

degradation and inducing a chemical hypoxia. In this thesis, cells were treated for 4 hours with 450 µM of $CoCl_2$ or 4 hours with 1mM of DMOG.

4.3 PROTEIN DETECTION

4.3.1 Homogenization

In order to study the protein levels of mice tissue lysates and cells with western blot analysis, the tissue and cells were homogenized to create a homogenous sample with soluble proteins. The mice colon was removed from the body, washed in cold 1 x PBS, emptied from feces, and cut open longitudinally and the epithelium was scraped of, or the colon was cut into smaller pieces (~50 mg). A piece/scraping was placed in a Potter-Elvehjem tissue grinder together with homogenization buffer (**11 Appendix**), 1 x protease inhibitor (PI)-cocktail (Roche, Basel, Switzerland) and 2 % Phenylmethylsulfonyl fluoride (PMSF) (Sigma-Aldrich). The piston was moved up and down (~75 times) until the tissue was close to completely dissolved, whereafter the sample was moved to an eppendorf tube (Eppendorf, Hamburgh, Germany) and heated for 5 minutes at 95 °C. The sample was then passed through a 25 G needle (BD, NJ, USA) 10 times followed by a 27 G needle 10 times to further homogenize the sample, shear the DNA, and to remove any excess pieces of tissue. Samples were stored at -80 °C.

The homogenization of cells started with washing the cells 3 times with 1 x PBS, adding 200 µl of homogenization buffer and scraping the cells off their plate using a pipette tip or a cell scrape. The sample was then moved to an eppendorf tube and heated for 5 minutes at 95 °C, after which the lysate was passed through a 27 G needle 10 times and stored at -80 °C.

4.3.2 BCA protein assay

BCA protein assay is used to determine the protein concentration of an acquired sample in order to dilute samples to a comparable concentration. The

reaction occurring in the assay is divided into two steps; in the first step proteins found in the sample of interest reduce Cu^{2+} ions to Cu^{1+} ions and in the second step bicinchoninic acid binds to Cu^{1+} ions creating a complex that absorbs light at 562 nm. This means that the amount of proteins found in the sample is proportional to the amount of Cu^{1+} in complex with bicinchoninic acid.

In this method, the samples obtained from homogenization were boiled for 5 minutes at 95 °C, vortexed, centrifuged for a few seconds and placed on ice. The samples were diluted 1:10 in MQ water and 25 µl of each sample was placed in triplicate in a 96-hole plate together with a control (homogenization buffer diluted 1:10 with MQ water) and known protein standards of bovine serum albumin (BSA) (50, 100, 250, 500, 750 and 1000 µg/ml) (Thermo Fisher, MA, USA). Reagents A and B from the BSA protein assay kit (Thermo Fisher) were mixed 50:1 and 200 µl of this solution was added to each well. The plate was gently shaken by hand and then incubated for 30 minutes at 37 °C. Thereafter, the plate was cooled down at RT and the absorption at 562 nm of each well was measured using the Victor 1420 photometer (Perkin Elmer, MA, USA). From the results of the BSA protein standards a standard curve was made, from which the concentration of each sample was determined. The samples were then boiled for 3 minutes at 95 °C, whereafter they were diluted in a 3 x Laemmli buffer (**11 Appendix**) to a concentration of 5 or 10 µg/10µl.

4.3.3 SDS-PAGE

A gel was casted from a 10 %, respectively 7 % acrylamide Running gel (**11 Appendix**) and 4,5% acrylamide Stacking gel (**11 Appendix**). The function of the stacking gel is to allow all samples and all sized proteins to have the same starting point, i.e., at the beginning of the running gel where the separation happens. The theory behind the even separation of proteins in the stacking gel is that a lower percentage of acrylamide leads to bigger pores in the gel, making it easier for all sized proteins to pass through. The second reason is that it has a lower pH level, which results in a low glycine dissociation. This

leads to proteins moving between a front of chloride ions and glycine molecules, leading to a homogenous pull through.

After the gel had polymerized, the gels were mounted into the run holder, which was placed in a buffer tank, and both were filled up with 1 x Running Buffer (**11 Appendix**). The sodium dodecyl sulfate (SDS) found in the running buffer and in the gel has the effect of disrupting the tertiary structure together with β-mercaptoethanol found in the sample buffer by breaking non-covalent and disulfide bonds and neutralizing the internal charge by coating the protein with negative charge. This allows for a fair separation of proteins according to their size only, with smaller proteins moving through the gel faster. In the next step, the wells in the gel were loaded with various protein samples (5 or 10g/10µl) and an iBright Prestained protein ladder (Thermo Fisher) (4µl), that was later used to estimate the sizes of separated proteins. After the gel was loaded with samples it was connected to a power source and ran at RT, 100-125 V, until the blue line had reached the end of the gel (approximately 1.5 hours).

4.3.4 Transfer

After running the gel, the proteins were transferred to a polyvinylidene difluoride (PVDF) membrane (Thermo Fisher). A sandwich was first constructed, by adding a sponge pad, 3 Whatman filter papers (Cytiva, MA, USA), an activated (1 min in methanol) PVDF membrane, the gel, a second sponge pad and finally 3 more Whatman filter papers.

The supporting grid (cassette) around the sandwich was closed and placed in a run holder, with the membrane facing the positive pole, in a buffer tank that was filled up with 1 x Transfer Buffer (**11 Appendix**) and a pack of ice to maintain the temperature during the run. The tank was then connected to a power source and ran at 100 V for 1 hour at 4 °C. After the run, the membrane was washed in PBS- 0.2% Tween (PBS-T) and the protein ladder was marked with a pen to help future analysis.

4.3.5 Western blot analysis

The PVDF-membrane from the previous step was blocked with a blocking buffer (PBS-T with 5 % milk powder) for 1 hour at RT on an oscillator. During this step, the open spots for protein attachments on the membrane are blocked, thus, reducing the chances of unspecific binding of antibodies, which otherwise leads to increased background detection.

After blocking the membrane was washed 3 times 5 minutes with PBS-T and thereafter incubated with a primary antibody (diluted in 0.5% BSA and 0.02% NaN3) (see **Table 2.**) overnight at 4 °C. Next day the membrane was washed 3 times 5 minutes with PBS-T and incubated with a secondary antibody (diluted in blocking buffer) (see **Table 2.**) for 1 hour at RT. After incubation with the secondary antibody the membranes were again washed 3 times 5 minutes with PBS-T, after which the protein bands of interest were visualized using iBright (Thermo Fisher).

Table 2. Primary and secondary antibodies used for Western blot analysis.

1^o Antibody	Dilution from stock	2^o Antibody	Dilution from stock
Rabbit anti-HIF-1α Cell signaling (36169s)	1:1000	Anti-Rabbit Promega (W401B)	1:10000
Rat anti-K8 DSHB (Troma I)	1:1000	Anti-Rat Alexa Fluor 680 Invitrogen	1:10000
Mouse anti-K18 Progen (61028)	1:1000	Anti-Mouse Alexa Fluor 800 Invitrogen	1:10000
Rat anti-K19 DSHB (Troma III)	1:1000	Anti-Rat Alexa Fluor 680 Invitrogen	1:10000
Mouse anti-K19 426	1:1000	Anti-Mouse Alexa Fluor 800 Invitrogen	1:10000
Rabbit anti-mTOR Cell signaling (2983s)	1:1000	Anti-Rabbit Promega (W401B)	1:10000
Rabbit anti-Phospho-4EBP1 Cell signaling (2855s)	1:1000	Anti-Rabbit Promega (W401B)	1:10000
Rabbit anti-4EBP1 Cell signaling (9644s)	1:1000	Anti-Rabbit Promega (W401B)	1:10000
Rabbit anti-Phospho-S6K Cell signaling (4858s)	1:1000	Anti-Rabbit Promega (W401B)	1:10000
Rabbit anti-S6K Cell signaling (2217s)	1:1000	Anti-Rabbit Promega (W401B)	1:10000
Mouse anti-β-tubulin Sigma-Aldrich (T8328)	1:1000	Anti-Mouse Alexa Fluor 800 Invitrogen	1:10000

4.4 RNA DETECTION

4.4.1 RNA isolation

Macherey-Nagel (PA, USA) RNA isolation kit was used for RNA isolation. A 10-30 mg piece of mouse colon was homogenized in 350 µl of RA1 buffer together with 3.5 µl of B-mercaptoethanol (Sigma-Aldrich) using the Tissueruptor (Qiagen, Hilden, Germany). The homogenized sample was then placed in a Nucleospin filter (in a collection tube) and centrifuged 1 min at 110000 x g. Thereafter the filter was discarded and 350 µl of ethanol (70 %) was added and the mixture was pipetted 5 times to further homogenize the lysate. The lysate was then loaded to a Nucleospin RNA column and centrifuged for 1 minute at 11000 x g. Next, 350 µl of MDB was added to the column and it was centrifuged for 1 minute at 11000 x g to dry the membrane. To digest and get rid of DNA, 95 µl of rDNase reaction mixture was added to the center of the column and incubated in RT for 15 minutes.

To then wash away digested DNA, 200 µl of RAW3 buffer was added to the column and centrifuged 30 seconds at 11000 x g, then the column was placed in a new collection tube and 600 µl of RA3 buffer was added and centrifuged for 30 seconds at 11000 x g. Finally, the flow through was discarded and 250 µl of RA3 buffer was added and centrifuged for 2 minutes at 11000 x g. To extract the RNA, the column was placed in a nuclease free collection tube, 50 µl of RNase-free water was added and centrifuged for 1 minute at 11000 x g. The RNA concentration and quality was then measured using Nanodrop (Thermo Fisher) and the samples were stored at -80 °C.

4.4.2 Complementary DNA synthesis

In order to detect the RNA from the RNA isolation it first has to be converted to complementary DNA (cDNA), i.e., a DNA segment formed by reverse transcriptase from RNA. For each isolated RNA sample 1 µg of RNA was diluted to a final volume of 11 µl with water, and then 1 µl of Oligo dT

oligonucleotide Primers (Promega, WI, USA) was added and the samples were incubated 5 minutes at 70 °C to denature the secondary structure. After the incubation the samples were placed on ice for 5 minutes to anneal primers to the RNA. To each sample was then added 5 µl od M-MLV RT 5 x reaction buffer (Promega), 1.25 µl of dNTP mix (10 mM) (Promega), M-MLV RT polymerase (200 U/µl) (Promega) and 5.75 µl of sterile water (Lonza, Basel, Switzerland). Thereafter the samples were incubated for 10 minutes at 40 °C, followed by 50 minutes at 43 °C and finally for 15 minutes at 70 °C. The cDNA was then diluted 1:4 with sterile water and stored at -20 °C.

4.4.3 Quantitative PCR

qPCR is a method where cDNA is amplified and detected by the binding of fluorescent molecules (SYBR green) to the amplified DNA. This is done to be able to compare the fold change of the fluorescent signals between samples, directly correlating to the amount of RNA produced from a gene of interest.

This method starts by preparing a mastermix for each gene of interest. The mix for one well contained 1) 5 µl of SensiFast SYBR Hi-ROX (Meridian Biosciences, OH, USA) 2) 0.3/0.4 µl of 10 µM Forward primer 3) 0.3/0.4 µl of 10 mM Reverse primer and 4) 2.2/ 2.3 µl of sterile water. For each well (94-well plate) 8 µl of mastermix together with 2 µl of sample was applied and the plate was covered with a plastic seal, centrifuged for 30 seconds at 1000 x g and ran with QuantStudio 3 PCR system (Thermo Fisher). See Table 3. For the sequence of primers used.

Table 3. Mouse primers used for qPCR.

Gene	Manufacturer	Sequence
HIF-1α	KAPA	5'-GCA CTA GAC AAA GTT CAC CTG AGA-3' 5'-CGC TAT CCA CAT CAA AGC AA-3'
VEGF-A	KAPA	5'-GCA GCT TGA GTT AAA CGA ACG-3' 5'-GGT TCC CGA AAC CCT GAG-3'
Bcl2	KAPA	5'-AGT ACC TGA ACC GGC ATC TG-3' 5'-GGG GCC ATA TAG TTC CAC AAA-3'
β-actin	KAPA	5'-TGG CTC CTA GCA CCA TGA AGA-3' 5'-GTG GAC AGT GAG GCC AGG AT- 3'

4.5 IMMUNOFLUORESCENCE STAINING

4.5.1 Immunofluorescence staining of cells

Cells grown on coverslips were washed 2 times with PBS to remove any excess media, and fixed with 4% paraformaldehyde (PFA) for 10 minutes at RT. PFA covalently cross-links proteins in the cells and on their membrane to create an insoluble network that will not wash away during the staining, thus, keeping everything intact until imaging. After fixation the coverslips with cells were moved to a humidifying chamber and washed 3 times 3 minutes with PBS-Triton X-100 (0.025%), whereafter they were incubated for 5 minutes with NP-40 (Applichem, Darmstadt, Germany) to permeabilize the cell membrane and allow passage for antibodies.

After permeabilization the cells were washed 3 times 3 minutes with PBS-Triton X-100 (0.025%), whereafter they were blocked with 2.5 % BSA (in PBS) for 20 minutes, followed by a second blocking with 2.5 % BSA + 2% Donkey and Goat serum for 20 minutes. The blocking solution was discarded and 1 antibody (See Table 4.) was added followed by incubation overnight at 4°C. The next day, the cells were washed 3 times 5 minutes with PBS, blocked for 10 minutes with 2.5 % BSA + 2% Donkey and Goat serum, after which they were incubated with 2° antibody for 45 minutes (in dark). The cells were then washed 3 times 5 minutes with PBS. In the second wash DRAQ5 (1:500) (Cell signaling, MA, USA) was added to stain the DNA. Finally, the cells were

mounted to microscope slides (Menzel, Braunschweig, Germany) with Prolong Gold Antifade reagent (Thermo Fisher) and stored for 12 hours in RT in dark, after which they were moved to 4°C.

4.5.2 Immunofluorescence staining of organoids

Organoids grown on coverslips were washed 2 times with PBS and incubated with 4% PFA for 20 minutes. After fixation the organoids were washed 3 times 5 minutes with wash buffer (1 x PBS containing 0.2% Triton X-100 and 0.05% Tween), after which the coverslips with organoids were moved to a humidifying chamber and permeabilized with 1 x PBS- Triton X-100 (0.5%) for 20 minutes. They were then washed once with wash buffer and blocked with 2.5% BSA + 2% Donkey and Goat serum for 30 minutes. 1° antibody was added and incubated overnight at 4°C.

The following day, the organoids were washed 3 times 5 minutes with wash buffer, whereafter they were incubated with 2° antibody at RT for 1 hour and 30 minutes (in dark). The coverslips were washed once with PBS, whereafter the DNA was stained with DRAQ5 (1:500) for 15 minutes and finally washed 2 times 20 minutes with PBS. The organoids were mounted onto microscope slides with Prolong Gold Antifade reagent and stored 12 hours in dark at RT before moved to long term storage at 4°C.

Table 4. Primary and secondary antibodies used for immunostaining.

1^{o} Antibody	Concentration	2^{o}Antibody/Probe	Concentration
Rabbit anti-HIF-1α Cell signaling (D1S7W)	Cells 1 to 500 Organoids 1 to 300	Goat anti-Rabbit Alexa Fluor 488 Invitrogen	1 to 200
		Phalloidin-Alexa Fluor 546 conjugate Invitrogen	1 to 250
		DRAQ5 Cell signaling (4084)	1 to 1000

4.5.3 Image acquisition

Stained organoids and cells were visualized using a confocal microscope (Leica TCS SP5 HCS A, Leica Microsystems, Wetzlar, Germany) with a 63x (organoids), and a 100x (cells) objective. The images were captured with a resolution of 1024 x 1024, a scanning speed of 600 Hz and a frame average of 4. All channels were set and held at the same laser power, gain and offset when analyzing samples from one series of staining.

4.6 COMPLEX IMMUNOPRECIPITATION

Protein complex immunoprecipitation is a method used to analyze the connection and complex formation between two or more proteins. The method uses antibodies specific for the protein of interest. The antibodies bound to their antigens and their possible complex bound proteins will then be extracted from the sample solution by a series of washes and with the help of magnetic beads. Finally, the extracted solution will be analyzed with western blot analysis for successful precipitation of the antigen/protein of interest, and for proteins bound in the complex.

First, two plates of Caco-2 cells were treated for 4 hours with of 200 µM $CoCl_2$ to induce hypoxia since complex formation with HIF-1α was probed. The plates were then emptied of media and 400 µl of PBS was applied to each plate, which were then scraped to collect all cells. Next, the collected cells were moved to an eppendorf tube and centrifuged 800 x g for 5 minutes. The supernatant was removed, and the cell pellet was resuspended in 1.5 ml Lysis Buffer (**11 Appendix**) + 0.5 mM of dithiothreitol (DTT) (gift from Meinander Lab) + 1 x PI-cocktail and 0.5 mM PMSF. The solution was homogenized with a 27 G needle and incubated on ice for 45 minutes (vortexed every 15 minutes).

After the incubation the sample was centrifuged at 1000 x g for 5 minutes, and the supernatant was divided into 1) Input (50 µl) 2) No antibody (600 µl) and

3) Immunoprecipitation (600 µl). The input was diluted 1:2 with a 3 x Laemmli buffer (without β-mercaptoethanol). Thereafter, 5 µl of anti-K18 (L2A1) (gift from Omary Lab) antibody was added to the 3) Immunoprecipitation sample and both 2) No Antibody and 3) Immunoprecipitation were put on rotation overnight at +4 °C.

Next day A/G magnetic beads (Thermo Fisher) (30 µl/ tube) were washed 3 times with 0,1% PBS-T solution. The beads were then mixed in with 2) No antibody and 3) Immunoprecipitation and they were left on rotation for another 20 minutes, allowing the beads to bind to the antibodies. The samples together with the beads were then washed 3 times with TEG buffer (**Appendix**) + 0.5 mM DTT + 1x PI and 0.5 mM PMSF, whereafter the beads were mixed in 40 µl of 3 x Laemmli Buffer (without β-mercaptoethanol) and boiled for 5 minutes at 95°C. All samples were stored at -20 °C.

4.7 QUANTIFICATION AND STATISTICAL ANALYSIS

4.7.1 Protein quantification

Western blot images acquired from iBright were imported to data software ImageJ. In the software, the intensity of the protein band of interest and the band for the housekeeper protein was measured for each sample and the measurements were imported to Excel (Microsoft, WA, USA). The fold change was calculated by first dividing the intensity of each protein band with that of the housekeeper loading control intensity, after which each value was divided by the average of the control group. Finally, student's t-test was conducted to look for significant differences between groups. In graphs, * = $p<0.05$, ** = $p<0.01$ and *** = $p<0.001$.

4.7.2 RNA quantification

The RNA results were calculated from the Ct-values of the target gene and the housekeeper gene using the delta-delta-Ct method (Equation 1.). The method

does not use any standards; thus, the results are presented as relative fold gene expression rates. From the results acquired a student's t-test was conducted.

$$\Delta Ct = Ct(\text{Target gene}) - Ct(\text{Housekeeper gene})$$

$$\Delta\Delta Ct = \Delta Ct(\text{Sample}) - \Delta Ct(\text{Control average}) \quad [1]$$

$$\text{Relative fold change} = 2^{-\Delta\Delta Ct}$$

4.7.3 Image quantification

The microscope images to be analyzed were imported to ImageJ (MD, USA) and the channels were split. Using the ROI manager and the nuclear channel, nuclei were identified and marked with the freehand tool and added as ROIs. The channel was then switched to the channel for HIF-1α, and the saved ROIs were added to the channel (**Figure 9.**). Then the intensity to area was calculated for each ROI and the results were imported to excel where a student's t-test was performed to look for any significant differences.

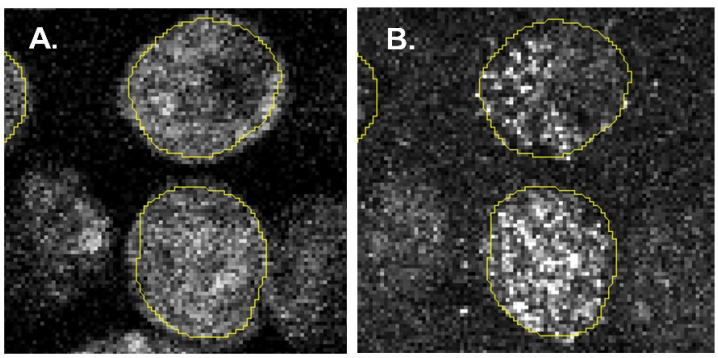

Figure 9. Image quantification. (A) The nuclear channel (DRAQ5) is used to create several ROIs surrounding the nucleus. **(B)** The ROIs are moved to the channel of interest, here HIF-1α, and the intensity to area for each ROI is measured.

5 RESULTS

5.1 The colon of K8$^{-/-}$ mice express higher levels of HIF-1α

Previous experiments using a PET hypoxia-tracer ([^{18}F] EF5) have indicated that K8$^{-/-}$ mice display significantly higher levels of hypoxia in the colon compared to K8$^{+/+}$ mice (**Supplemental figure 1.**). Therefore, to further investigate a potential causality between K8 loss and hypoxia signaling a western blot analysis of the protein levels of the hypoxia-related transcription factor HIF-1α was conducted on K8$^{-/-}$ mice. The results indicate that HIF-1α is significantly upregulated in the colon of K8$^{-/-}$ mice compared to K8$^{+/+}$ mice (**Figure 10.A-B.**).

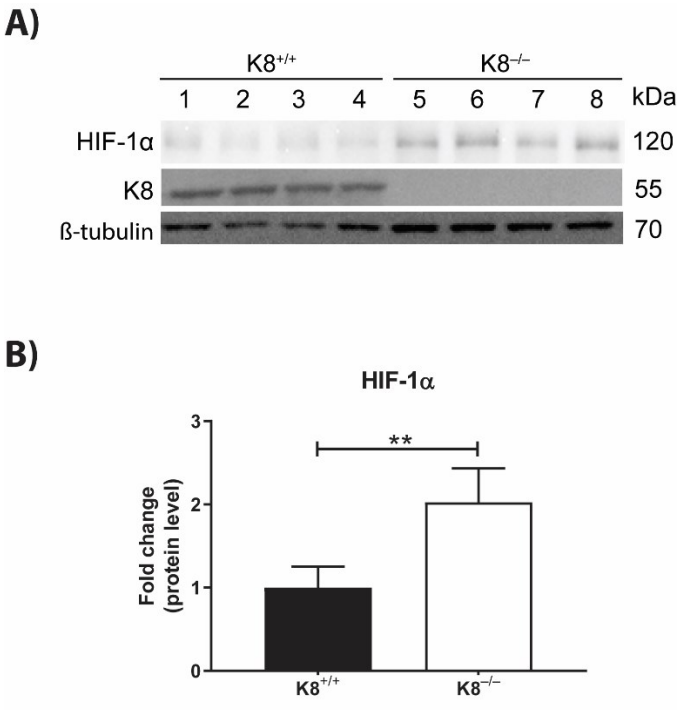

Figure 10. Upregulated protein levels of HIF-1α in K8$^{-/-}$ mice. (A) Western blot analysis of HIF-1α and K8 levels in K8$^{+/+}$ (wells 1-4) and K8$^{-/-}$ (wells 5-8) mice (n=4) colon total lysates. **(B)** A fold change comparison of HIF-1α levels in K8$^{+/+}$ and K8$^{-/-}$ mice calculated from western blot analysis data from A. Protein levels were normalized to β-tubulin. Bars illustrate the mean fold change (n=4) and error bars

illustrate the standard deviation (SD). Statistical significance was calculated with student's t-test where ** = $p<0.01$.

To further analyze that the K8-loss induced HIF-1α increase was dependent on the K8 loss, a time course deleting K8 in the colon epithelium was conducted (**Supplemental figure 2.**). K8 was gradually erased using a tamoxifen induced deletion in $K8^{flox/flox}$; Villin-$CreER^{t2}$ mice. Average HIF-1α levels started increasing despite large fluctuations during the 14 days analyzed and reached significantly higher levels on day 5 and 12 (compared to day 0), however, after 14 days no significant difference could be detected. For HIF-1αs target gene, VEGF, the mRNA fluctuated and reached significantly lower levels on day 6 (compared to day 0), whereafter it reached a non-significant level at day 14.

5.2 HIF-1α is not upregulated because of intestinal inflammation in $K8^{-/-}$ mice

An activated hypoxia pathway and increased levels of HIF-1α have been noticed in colitis mouse models and human IBD patients, indicating that HIF-1α is upregulated as a response to inflammation (Shah, 2016). To investigate whether inflammation is the cause of our observed HIF-1α upregulation, mice were treated with antibiotics to ameliorate the colon inflammation. The protein levels of HIF-1α remained increased in antibiotics treated $K8^{-/-}$ mice compared to $K8^{-/-}$ baseline mice (p= 0.97) (**Figure 11.A.**).

Moreover, young mice (2-3 days old), which show no colon inflammation (Toivola et al., 2004), were analyzed for HIF-1α in the colon. In accordance with the antibiotic treated mice, the results indicate that $K8^{-/-}$ mice had increased levels of HIF-1α compared to $K8^{+/+}$ mice (**Figure 11.B-C.**). In conclusion the upregulated HIF-1α protein levels are not caused by colon inflammation.

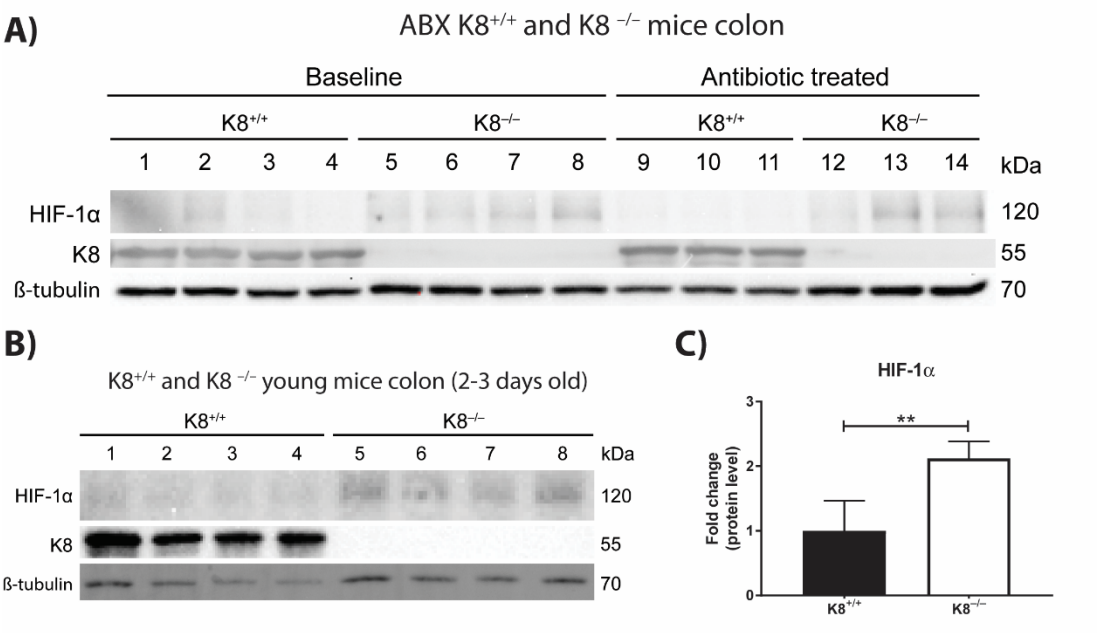

Figure 11. K8$^{-/-}$ HIF-1α upregulation is inflammation independent. (A) Western blot analysis of HIF-1α and K8 levels of crudely isolated colon epithelium lysates from K8$^{+/+}$ and K8$^{-/-}$ mice (n=3) (antibiotics treated/ABX). **(B)** Western blot analysis of HIF-1α and K8 in colon total lysates from young K8$^{+/+}$ (wells 1-4) and K8$^{-/-}$ (wells 5-8) mice (n=4) (2-3 days old). **(C)** Fold change comparison of HIF-1α levels from figure B. Protein levels were normalized to β-tubulin. Bars represent mean fold change (n=4) with SD error bars. Statistical significance was calculated with student's t-test where ** = $p<0.01$.

5.3 PI3K/Akt/mTOR pathway is hyperactive in K8 conditional knockout mice, but does not cause a difference in HIF-1α target gene expression

Studies show that keratins are part of the regulation of Akt via unknown mechanisms (Ku et al., 2010; Habtezion et al., 2011). To understand the mechanism behind the upregulation of HIF-1α and the possible regulation via Akt, we investigated the oxygen-independent hypoxia pathway, which is the PI3K/mTOR/Akt pathway. Firstly, the results show that K8$^{flox/flox}$;Villin-Cre have higher levels of HIF-1α, thus, indicating that the effect seen is colon and K8 specific. Furthermore, the results show that K8 conditional knockout mice, K8$^{flox/flox}$;Villin-Cre, have a more active pathway compared to K8$^{flox/flox}$ mice (wild type), where mTOR targets 4E-BP1 and S6K have been

hyperphosphorylated. Lastly, a slight increase in mTOR protein levels can be observed. (**Figure 11.A-B.**)

To further study if mTOR is part of the upregulation of HIF-1α, $K8^{flox/flox}$ and $K8^{flox/flox}$;Villin-Cre colon organoids were treated with rapamycin, an inhibitor of mTOR. In $K8^{flox/flox}$ organoids, the protein level of HIF-1α was completely erased after 2 hours of rapamycin treatment, whilst in $K8^{flox/flox}$;Villin-Cre organoids the rapamycin treatment reduced the levels of HIF-1α, however, low concentrations could still be detected, suggesting a hyperactive mTOR (**Figure 11.C.**).

Lastly, the mRNA levels of HIF-1α target genes were studied to further investigate the effect of the K8 deletion-induced increase in HIF-1α and the hyperactive upstream signaling. The results show that there was no significant difference in the amounts of HIF-1α and its target genes VEGF and Bcl2 when comparing the mRNA levels between $K8^{flox/flox}$ and $K8^{flox/flox}$;Villin-Cre mice (**Figure 11.D.**).

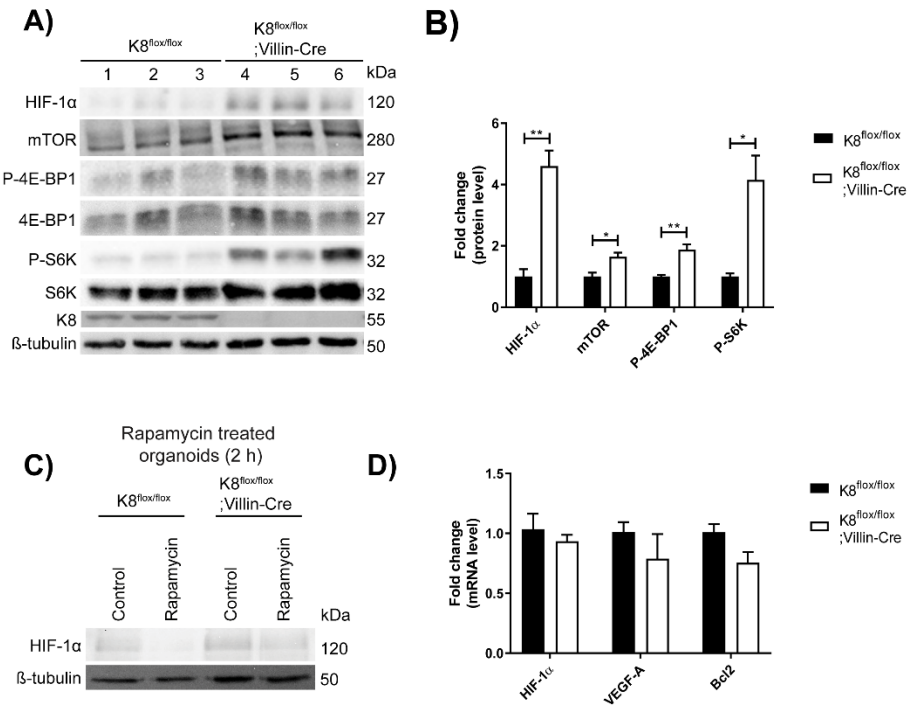

Figure 12. K8 deletion leads to a hyperactive mTOR pathway, but no change in HIF-1α target gene expression. (A) A western blot analysis of HIF-1α, mTOR, P-4E-BP1, 4E-BP1, P-S6K, S6K and K8 levels of crudely isolated colon epithelium lysates from $K8^{flox/flox}$ (wells 1-3) and $K8^{flox/flox}$;Villin-Cre (wells 4-6) mice (n=3). **(B)** The fold change comparison of proteins analyzed in figure A. Protein levels were normalized to β-tubulin (HIF-1α and mTOR), 4E-BP1 (P-4E-BP1) and S6K (P-S6K). The bars represent mean fold change (n=3) with SD error bars **(C)** HIF-1α western blot analysis of $K8^{flox/flox}$ and $K8^{flox/flox}$;Villin-Cre colon organoids (n=1) treated with 100 nM rapamycin for 2 hours. **(D)** Relative fold change comparison of HIF-1α, VEGF and Bcl2 mRNA levels in $K8^{flox/flox}$ and $K8^{flox/flox}$;Villin-Cre mice (n=3) colon total lysates. mRNA levels were normalized to β-actin. Bars represent mean fold change (n=3) with SD error bars. Statistical significance was calculated with student's t-test where * = $p<0.05$ and ** = $p<0.01$.

5.4 Elevated HIF-1α levels in *in vitro* and *ex vivo* models with K8 deletion

To further test the hypothesis that K8 to some extent regulates or influences the hypoxia pathway, a series of tests were conducted *in vitro* and *ex vivo* to see if the same effect seen before can be replicated. This experiment used K8/K18 siRNA Caco-2 cells, K8 CRISPR/Cas9 cells and $K8^{flox/flox}$;Villin-Cre organoids. Compared to control Caco-2 cells (Mock), K8/K18 siRNA Caco-2 cells had slightly but significantly higher levels of HIF-1α (**Figure 13.A-B.**). The same phenomenon could be recognized in $K8^{-/-}$ CRISPR/Cas9 cells treated with HIF-1α stabilizing agent $CoCl_2$ for 4 hours, where there is a significant increase in HIF-1α compared to $K8^{+/+}$ CRISPR/Cas9 cells (**Figure 13.C-D.**).

Lastly, as seen in **Figure 12.C** the $K8^{flox/flox}$;Villin-Cre colon organoids had higher protein levels of HIF-1α in control conditions during normoxia compared to $K8^{flox/flox}$ organoids, therefore this experiment was designed to test if the same outcome is applicable in hypoxia. The results in **Figure 13.E** indicate that $K8^{flox/flox}$;Villin-Cre organoids grown for 16 hours in hypoxic conditions (1% oxygen) have higher levels of HIF-1α, compared to that of $K8^{flox/flox}$ organoids.

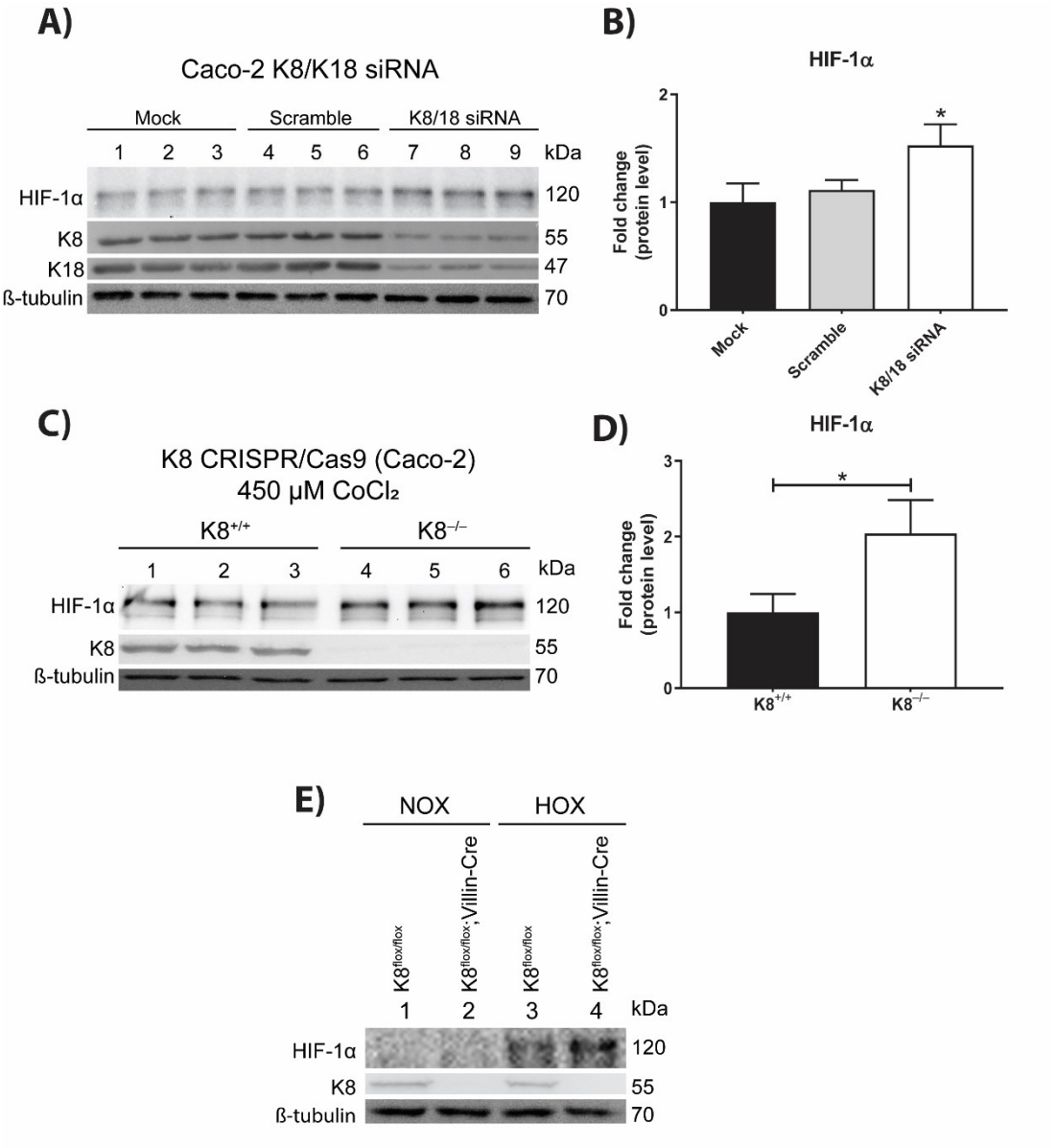

Figure 13. Higher levels of HIF-1α in *in vitro* and *ex vivo* models with K8 deletion. **(A)** Western blot analysis of HIF-1α, K8 and K18 protein expression in normoxia compared between Caco-2 Mock (wells 1-3)/ Caco-2 K8/K18 Scramble (wells 4-6), and Caco-2 K8/K18 siRNA treated cells (wells 7-9) (n=3). **(B)** Graph of protein quantification results from figure A. Protein levels were normalized to β-tubulin. Bars represent mean fold change (n=3) with SD error bars **(C)** Protein levels of HIF-1α and K8 in $K8^{+/+}$ CRISPR/Cas9 (wells 1-3) and $K8^{-/-}$ CRISPR/Cas9 (wells 4-6) Caco-2 cells (n=3) treated with 450µM $CoCl_2$ for 4 hours. **(D)** Graph of protein quantification results from figure C. Protein levels were normalized to β-tubulin. Bars represent mean fold change (n=3) with SD error bars **(E)** HIF-1α and K8 levels of $K8^{flox/flox}$ and $K8^{flox/flox}$;Villin-Cre organoids (n=1) that have been grown in normoxia (NOX, wells 1-

2) and 1% hypoxia (HOX, wells 3-4) for 16 hours. Statistical significance was calculated with student's t-test where * = $p<0.05$.

5.5 There is a physical association between K8/K18 and HIF-1α, either direct or indirect

To investigate whether there was a direct (or indirect) association between K8 and HIF-1α, a complex immunoprecipitation was conducted. Caco-2 cells were treated with 1 mM of DMOG to stabilize HIF-1α, lysed and incubated with K18 antibodies to eventually precipitate K18 and its binding partner K8. Lastly, the precipitated sample was analyzed for the potential binding of HIF-1α. The Caco-2 input sample (well 1), working as a control, indicates that there is HIF-1α in the lysed samples. Furthermore, the sample without the K18 antibody (well 2) shows no sign of HIF-1α and minor levels of K8/K18, in contrast to the sample incubated with K18 antibodies (well 3), which shows a HIF-1α band and high levels of K8/K18, indicating that K8/K18 is in complex with HIF-1α.

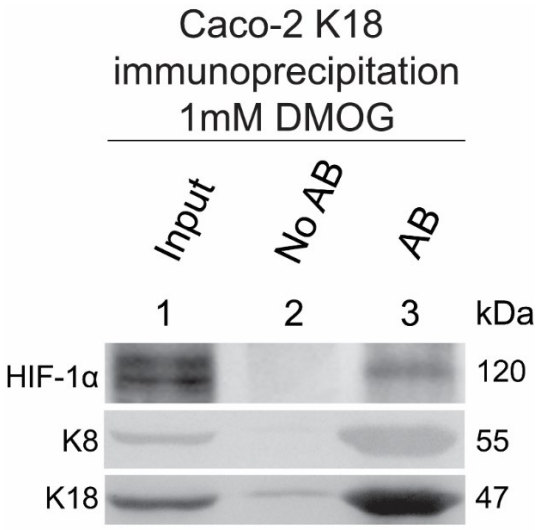

Figure 14. K8/K18 binds in complex with HIF-1α. HIF-1α, K8 and K18 western blot analysis of a K18 complex-immunoprecipitation on Caco-2 cells treated for 4 hours with 1mM DMOG. Located in well 1 is the input sample, in well 2 the sample with no antibody, and lastly in well 3 the sample incubated with K18 antibodies as bait. n=3.

5.6 Increased nuclear HIF-1α *in vitro* and *ex vivo* during normoxia

Results in this thesis have indicated a complex between K8 and HIF-1α (**Figure 14.**) and an increased activity of the hypoxia pathway in K8 knockout models (**Figures 10-13.**), however, no increase in HIF-1α target gene mRNA levels (**Figure 12.D.**). Thus, the next step was to look at the localization of HIF-1α in the models, more specifically the amount of HIF-1α in the nucleus. This was conducted by immunofluorescence staining *in vitro* and *ex vivo* models for HIF-1α and measuring the intensity of HIF-1α signal in the nucleus.

In the *ex vivo* organoid model grown in normoxia, there was a significant increase of HIF-1α in the nucleus of $K8^{flox/flox}$;Villin-Cre organoids compared to that of the $K8^{flox/flox}$ organoids. However, in the organoids grown in hypoxia (1%) for 16 hours no significant difference could be detected (**Figure 15. A-B.**). Furthermore, $K8^{flox/flox}$ organoids responded to hypoxia with an increase in HIF-1α signal in the nucleus compared to normoxia, whereas the $K8^{flox/flox}$;Villin-Cre organoids nuclear HIF-1α signal did not increase from normoxia to hypoxia. For the *in vitro* model grown in normoxic conditions, $K8^{-/-}$ CRISPR/Cas9 had a significantly higher signal of HIF-1α in the nucleus compared to $K8^{+/+}$ CRISPR/Cas9 cells. In hypoxia (1%) for 4 hours, no significant difference was found (**Figure 15. C-D.**). Both $K8^{+/+}$ CRISPR/Cas9 and $K8^{-/-}$ CRISPR/Cas9 cells responded to hypoxia with an increase of HIF-1α in the nucleus compared to normoxia.

A)

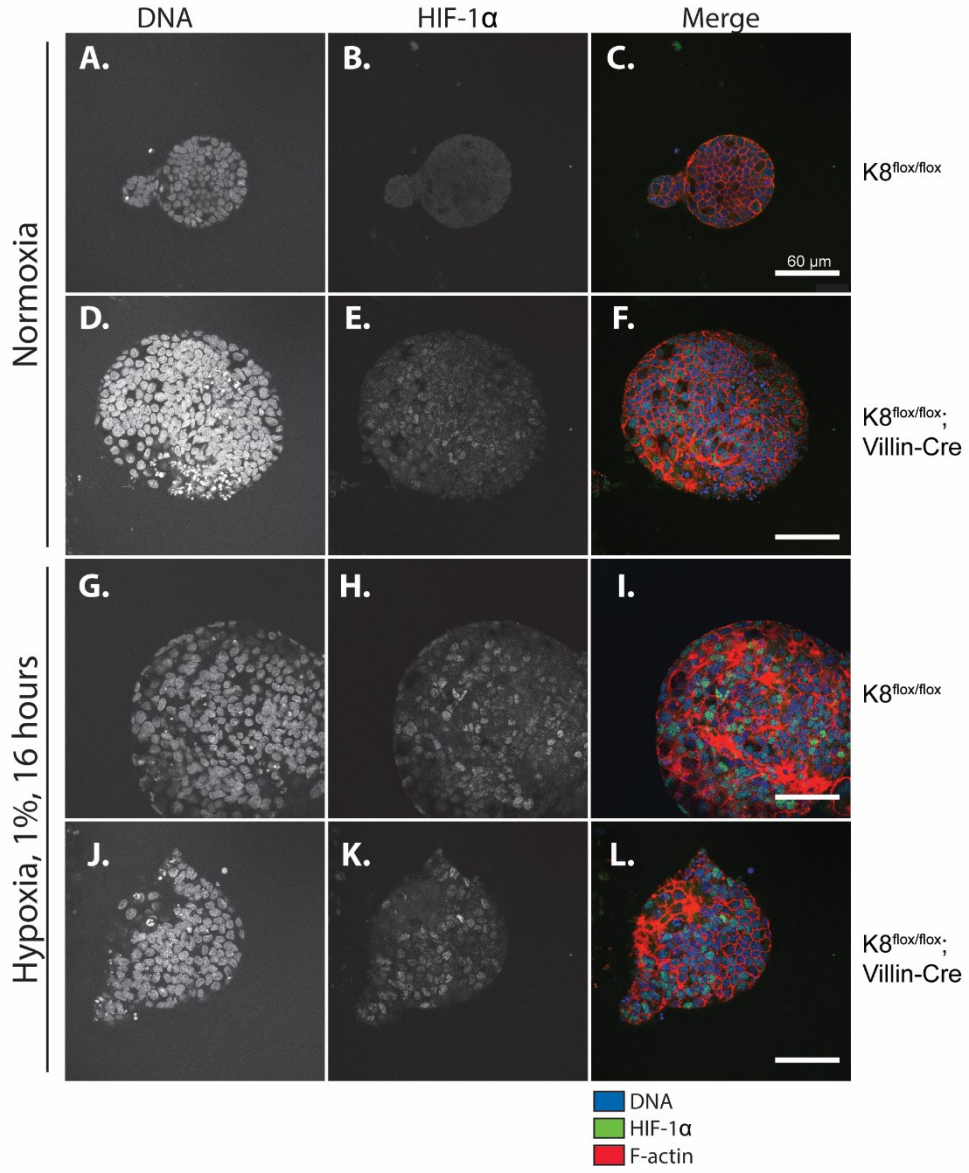
DNA
HIF-1α
Merge
A.
B.
C.
D.
E.
F.
G.
H.
I.
J.
K.
L.
Normoxia
Hypoxia, 1%, 16 hours
K8flox/flox
K8flox/flox; Villin-Cre
K8flox/flox
K8flox/flox; Villin-Cre
60 µm
DNA
HIF-1α
F-actin

B)

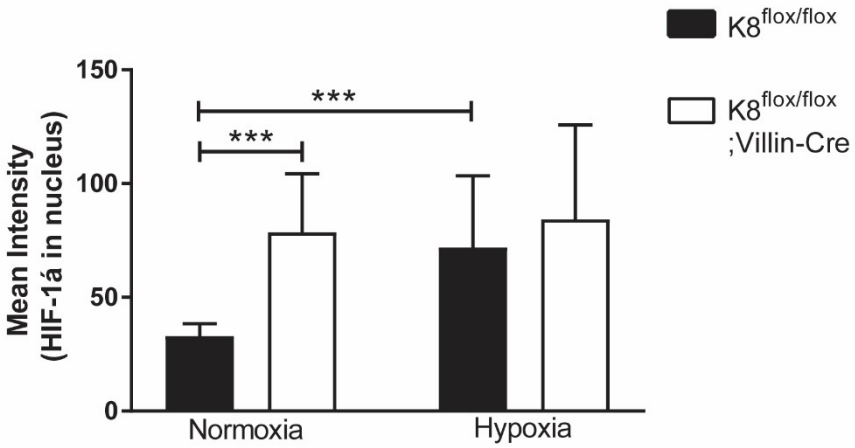
K8flox/flox
K8flox/flox ;Villin-Cre
Mean Intensity (HIF-1á in nucleus)
150
100
50
0
***
***
Normoxia
Hypoxia

C)

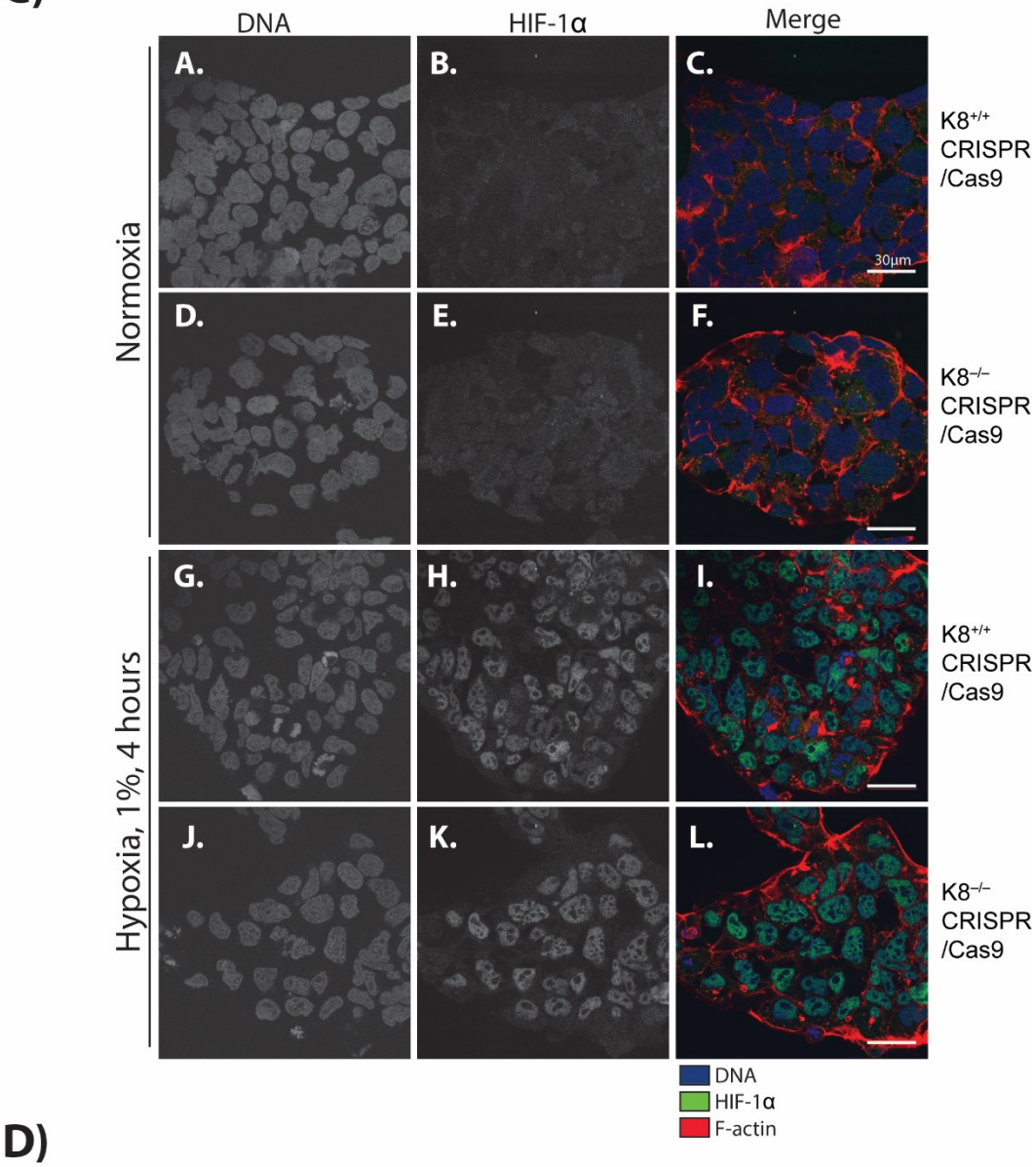
DNA
HIF-1α
Merge
A.
B.
C.
D.
E.
F.
G.
H.
I.
J.
K.
L.
Normoxia
Hypoxia, 1%, 4 hours
K8+/+ CRISPR /Cas9
K8−/− CRISPR /Cas9
K8+/+ CRISPR /Cas9
K8−/− CRISPR /Cas9
30μm
DNA
HIF-1α
F-actin

D)

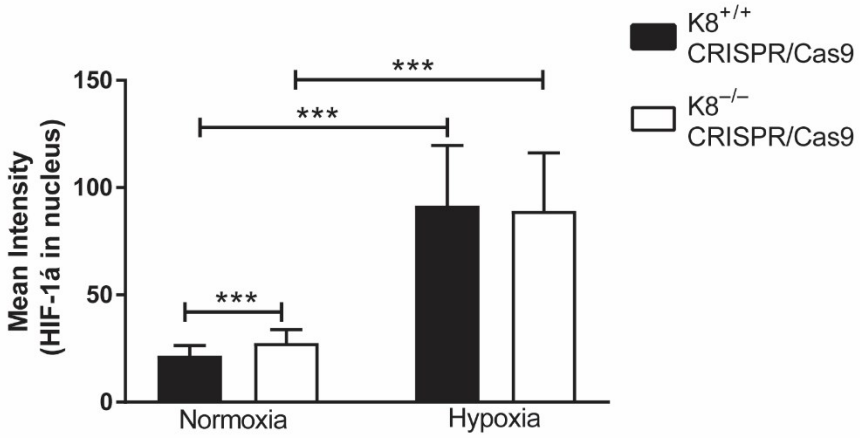
Mean Intensity (HIF-1á in nucleus)
150
100
50
0
***
***
***
Normoxia
Hypoxia
K8+/+ CRISPR/Cas9
K8−/− CRISPR/Cas9

Figure 15. In vitro and ex vivo experiments show increased nuclear HIF-1α in normoxia. (A) $K8^{flox/flox}$ and $K8^{flox/flox}$;Villin-Cre organoids were grown in normoxia (A.-F.) or in 1% hypoxia (G.-L.) and immunostained for DNA (blue), HIF-1α (green) and F-actin (red). **(B)** Quantification of mean intensity (n=41 nuclei) of HIF-1α signal in the nucleus of the cells in figure A., both during normoxia and after 16 hours of hypoxia (1%). Bars represent mean intensity with SD error bars. **(C)** $K8^{+/+}$ CRISPR/Cas9 and $K8^{-/-}$ CRISPR/Cas9 cells were grown in normoxia (A.-F.) or in 1% hypoxia (G.-L.) and immunostained for DNA (blue), HIF-1α (green) and F-actin (red). **(D)** Quantification of mean intensity (n=16 nuclei) of HIF-1α signal in the nucleus of the cells in figure C., both during normoxia and after 4 hours of hypoxia (1%). Bars represent mean intensity with SD error bars. Statistical significance was calculated with student's t-test where *** = $p<0.001$.

5.7 *In vitro* acute hypoxia does not affect keratin levels

Numerous studies of keratins have pointed out the importance of keratins in stress protection. Furthermore, Lähdeniemi et al. (**Supplemental figure 1. B.**) have shown that keratins are upregulated in mice after hypoxia treatment. Therefore, we wanted to investigate the same phenomenon *in vitro,* and look for more evidence of causality between hypoxia (exposure) and keratin regulation (outcome). To investigate this, Caco-2 cells were incubated 4 and 16 hours in hypoxia and the levels of keratins were quantified and compared against that of cells incubated in normoxia. Results show that after respective incubations there was a clear increase of HIF-1α, however, no significant difference in keratin levels could be detected (**Figure 16. A-C.**).

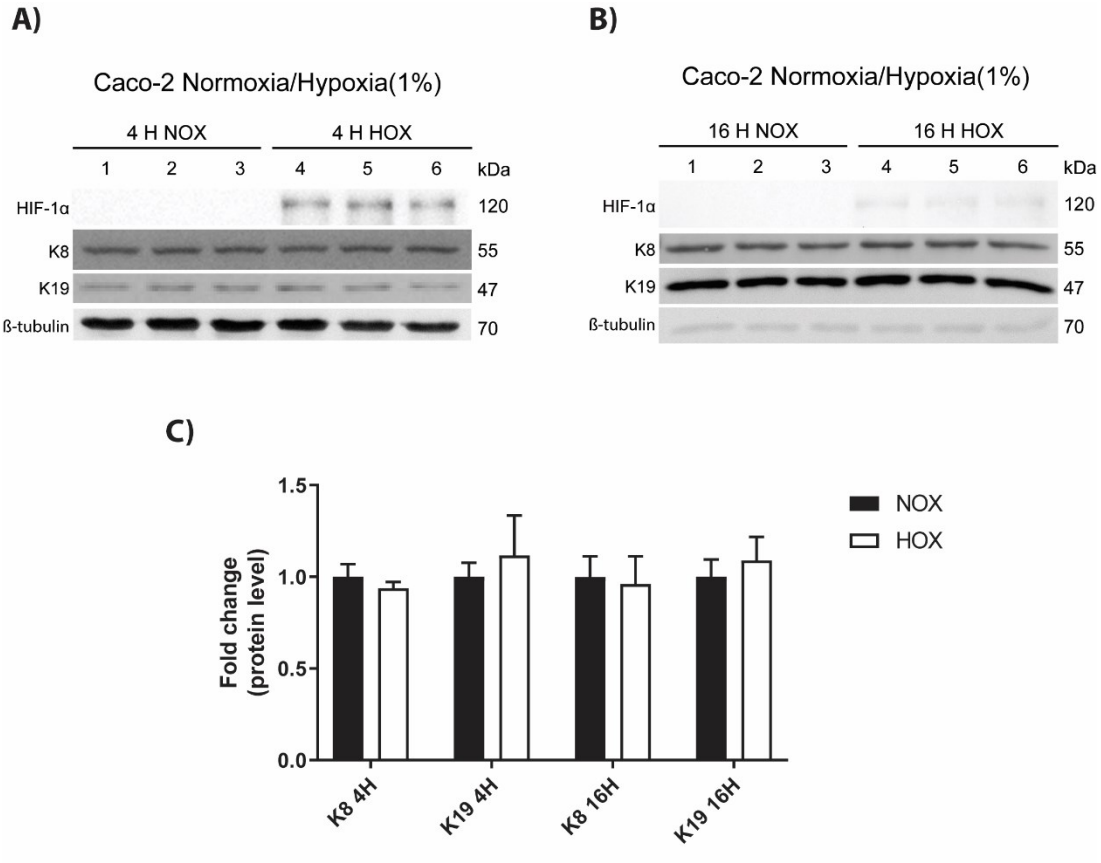

Figure 16. Keratin protein levels stay unaffected during hypoxia *in vitro*. (A) Caco-2 cells (n=3) were incubated 4 hours in normoxia (wells 1-3) and hypoxia (1%) (wells 3-6). Levels of HIF-1α, K8 and K19 were measured with western blot analysis. **(B)** Caco-2 cells (n=3) incubated 16 hours in normoxia (wells 1-3) and hypoxia (1%) (wells 3-6). HIF-1α, K8 and K19 were measured with western blot analysis. (**C**) Protein quantification graph comparing keratin levels between normoxic (NOX) and hypoxic (HOX) (4 hours and 16 hours) conditions. Protein levels were normalized to β-tubulin. Bars represent mean fold change (n=3) with SD error bars. Statistical significance was calculated with student's t-test.

6 DISCUSSION

6.1 Clear connection between K8 deletion and activated hypoxia pathway

As shown in **supplemental figure 1,** the colon of K8 $^{-/-}$ mice had a twofold uptake of the PET hypoxia-tracer [^{18}F] EF5. In this thesis, we noticed the same phenomenon where both K8$^{-/-}$ and K8$^{flox/flox}$;Villin-Cre showed significantly higher levels of the transcription factor HIF-1α compared to that of wild type mice, which suggests an activated hypoxia pathway (**Figure 10. and 12.**). Furthermore, it was successfully shown that the same phenomenon is also replicable *in vitro* and *ex vivo*, which strengthens the hypothesis that K8 is affecting the hypoxia signaling (**Figure 13.**).

At first thought, one would expect target mRNA to increase in pace with increased levels of their transcription factor. Interestingly, even though a clear connection between K8 loss and increased HIF-1α levels was established, the mRNA analysis of HIF-1α target genes showed no difference comparing K8$^{flox/flox}$ and K8$^{flox/flox}$;Villin-Cre mice (**Figure 12.D.**). It is possible that a prolonged expression of HIF-1α would result in a downregulation of the transcriptional activity, e.g., via p14^{ARF} and CITED2/CITED4 (Bárdos, Ashcroft, 2005; Horak et al., 2010). Another explanation for this could be that there are factors like chromatin-regulating proteins and chromatin modifications that are affecting the effectiveness of the transcription. Moreover, since HIF-1α has been shown to bind to roughly 500 sites and activate over 100 genes, it might be that there are other target genes that are activated, just not the ones we have investigated (Semenza, 2007; Schödel, Mole & Ratcliffe, 2013).

To prove that the effect seen is solely dependent on the loss of K8, K8 was gradually deleted in the colon epithelium of mice and HIF-1α levels were followed, as presented in **supplemental figure 2**. The levels of K8 decreased in a linear manner, however, HIF-1α levels fluctuated during the experiment,

after which it adapted to normal levels seen in wildtype mice. Initially, we thought the fluctuating HIF-1α was the result of a negative feedback mechanism, as described above (Bárdos, Ashcroft, 2005; Horak et al., 2010). With this knowledge we looked at the transcriptional activity, i.e., the levels of VEGF mRNA. VEGF reached a significantly lower level after six days, after which it adapted to normal levels. The most plausible explanation for the somewhat controversial results is that tamoxifen, which is a cancer drug known for lowering levels of many pro- cancerous compounds, would have down regulated HIF-1α protein and VEGF mRNA levels, and perhaps caused the fluctuations we saw (Garvin, Dabrosin, 2003; Yang et al., 2015; Cortes et al., 2019). In order to draw any conclusions from the experiment one would have to treat wildtype mice from the same mouse model with tamoxifen, creating a similar timeline, and from there look for any effects tamoxifen might have.

6.2 Keratins are affecting the hypoxia pathway through the PI3K/Akt/mTOR pathway

Knowing that K8 is to some extent influencing the hypoxia pathway we set out to investigate the cause of the effect. Previous studies have shown that K8/K18 interacts with Akt, and that K8 deletion can cause a hyperphosphorylation of Akt, thus, the focus was shifted to the PI3K/Akt/mTOR- pathway (Ku et al., 2010; Habtezion et al., 2011). As the results indicate (**Figure 12.**), S6K and 4E-BP1 have been hyperphosphorylated in $K8^{flox/flox}$;Villin-Cre mice, indicating an active mTOR that has most likely been activated as a result of Akt activity. To further examine that mTOR was responsible, organoids were treated with rapamycin, an inhibitor of mTOR. HIF-1α levels of $K8^{flox/flox}$ organoids were erased after treatment, whereas in $K8^{flox/flox}$;Villin-Cre organoids the levels were reduced, but not erased, suggesting the involvement of an hyperactive mTOR. Perhaps K8/K18 works as a phosphate sponge that can absorb some of the activating phosphorylations from Akt, and when K8 is knocked out the hyperphosphorylation is causing an increase in HIF-1α (**Figure 17. A.**) (Ku, Omary, 2006).

Furthermore, it was proven that HIF-1α is upregulated on a translational level by treating CRISPR/Cas9 cells with $CoCl_2$ (**Figure 13. C.**), which is a compound that interrupts the degradation pathway of HIF-1α. Since the degradation was stopped, or at least slowed down, and the $K8^{-/-}$ CRISPR/Cas9 cells had higher levels of HIF-1α compared to $K8^{+/+}$ CRISPR/Cas9 cells, the results strongly suggest that K8 deletion is responsible for increasing the translation of HIF-1α.

Considering the fact that hypoxia and HIF-1α has been associated with multiple colitis mouse models and also human IBD patients, where it protects the colon from damage, one could think that the upregulation of HIF-1α seen in our $K8^{-/-}$ mice is a consequence of the intestinal inflammation (Karhausen et al., 2004; Xue et al., 2013). However, we show here that young mice without any inflammation and older mice treated with antibiotics still appeared to have an upregulation of HIF-1α (**Figure 11.**). Moreover, $K8^{-/-}$ CRISPR/Cas9 Caco-2 colorectal cancer cells grown *in vitro*, that do not grow in an inflammatory environment, have an upregulation of HIF-1α (**Figure 13.C.**). These results strongly suggest that the effect we see is not a result of inflammation but linked to K8 loss. Studies do, however, show that the deletion of K8 in mice has caused a stress state, which leads to an increased production of cytokines (Habtezion et al., 2005). Therefore, we believe that cytokine upregulation could be another possible reason for the observed hyperactive PI3K/Akt/mTOR pathway. The hypothesis is that the increase in cytokines leads to activated RTKs, which further activate PI3K and RAS, leading to a cascade resulting in higher HIF-1α translation as previously described (**Figure 17.B.**). This thesis has focused on the PI3K/Akt/mTOR pathway; thus, it would be interesting in the future to also check for activity in the RAS/RAF/MEK/ERK pathway. If this pathway would follow the same pattern, with $K8^{-/-}$ resulting in over activation, the activation of the hypoxia pathway and the role of K8 could be explained as merely stress protectors, whose absence leads to an increase in cytokines and eventually upregulation of HIF-1α.

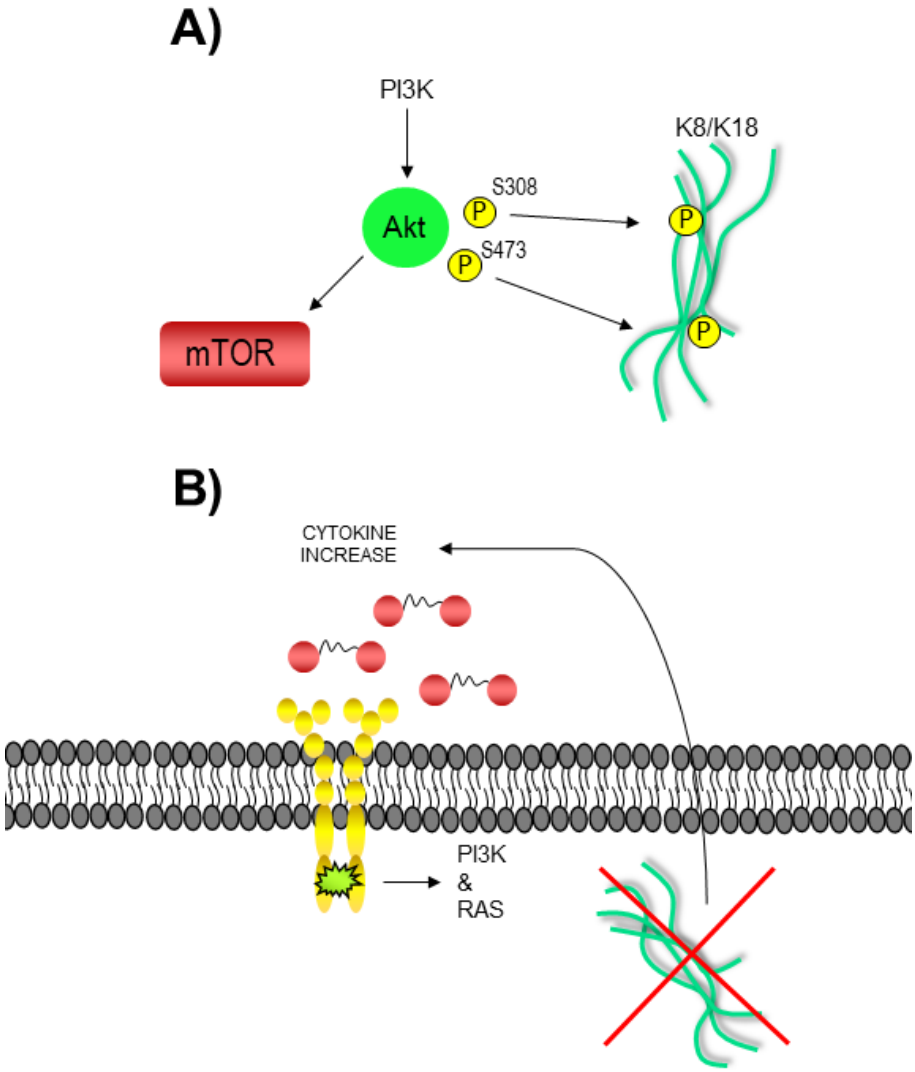

Figure 17. HIF-1α could be upregulated in K8$^{-/-}$ through lost Akt interactions or increased cytokine stimulation. These two illustrations show the possible mechanisms of HIF-1α upregulation in K8$^{-/-}$ models. **(A)** K8 and K18 heterodimer could work as a phosphor sponge that can absorb some of the phosphorylation that is activating Akt (S308 and S473), thus, downregulating the pathways activity. **(B)** Another possible mechanism of HIF-1α overexpression is through cytokines. Keratin loss could lead to increased cytokines, which activate RTKs, leading to an active PI3K/Akt/mTOR pathway and RAS/RAF/MEK/ERK pathway and increased HIF-1α translation.

6.3 Keratins might affect HIF-1α localization

An aim of this thesis was to determine if K8 affects HIF-1α localization. It was shown in this thesis that K8/K18 is in complex with HIF-1α when HIF-1α is stabilized, and studies show that K8/K18 also binds to other signaling molecules (Bragulla, Homberger, 2009). Thus, the hypothesis emerged that K8 would function as an anchor for HIF-1α, and its loss would lead to HIF-1α translocating into the nucleus. Furthermore, another hypothesis was that loss of keratins, which create structural integrity to the cell and interact with lamins in the nucleus, could lead to a more permeable nucleus that allows more entrance for molecules such as HIF-1α (Stenvall et al., 2020).

In optimal conditions, one would use *in vivo* models to investigate this aim, however, because of problems with antibodies in the staining process, this thesis used *in vitro* and *ex vivo* models (**Figure 15.**). For both $K8^{-/-}$ models grown in normal oxygen concentrations, a significant increase of HIF-1α in the nucleus of the cells could be recognized compared to $K8^{+/+}$ cells. There is a possibility that HIF-1α is translocated to the nucleus in greater amounts in $K8^{-/-}$ models in normoxia because of lost K8-HIF interactions or a more permeable nucleus, however, this could also be a result of higher basal levels of HIF-1α. The limit of this study is that there is no way to determine the actual mechanism for the observed outcome. As for hypoxic conditions, we show that $K8^{-/-}$ models indeed have a higher level of HIF-1α, however, there is no indication of HIF-1α being more localized into the nucleus of the $K8^{-/-}$ models. Since it is hypoxic conditions, it might be that the nuclear HIF-1α in both $K8^{+/+}$ and $K8^{-/-}$ models is saturated, or HIF-1α´s binding partner ARNT is saturated, so no difference is observed. Interestingly, in the *ex vivo* $K8^{flox/flox}$;Villin-Cre organoids the amounts of nuclear HIF-1α did not increase significantly from normoxia to hypoxia as one might expect. This could, however, be because of already the overexpressed HIF-1α levels and perhaps saturated nuclear HIF-1α levels as described above. For future studies, one would have to treat the cells and organoids with different levels of hypoxia and different exposure times, to investigate if those parameters would affect the results seen.

6.4 Keratins are not upregulated *in vitro* during hypoxia

Keratins function as stress cushions, absorbing mechanical or chemical stimuli the cells face. Toivola et al., (2010) described that keratin are upregulated in stress conditions, moreover, Lähdeniemi et al. (manuscript) showed that mice treated with hypoxia have an upregulation of keratins. Therefore, this thesis set an aim to test whether hypoxia-induced stress also would cause an upregulation of keratins *in vitro*, and if so, how much it would differ from normoxic conditions. The first experiment was conducted with Caco-2 cells subjected for 4 hours with 1% oxygen (**Figure 16. A.**), however, this did not cause any upregulation. The next step was to treat them for a longer period in case time would be a factor, thus, giving keratins some more time to adapt to the stress. However, after 16 hours of 1% oxygen (**Figure 16. B.**) the results stayed the same, with no upregulation.

There are a couple of possibilities for the results observed. Firstly, it might be that hypoxia does not affect keratins in cancer cells (*in vitro*), since they differ greatly from normal cells in many aspects, such as metabolism and signaling, which could affect the observed results. Furthermore, the results could be explained by the notable difference between cultured cells (2D) and mice in the regulation of cellular functions, where the cultured cells have very limited cellular and extracellular interactions compared to mice. Lastly, it might be that *in vitro* keratins adapt differently to hypoxic stress when subjected to a prolonged exposure to hypoxia, such as 24 hours demonstrated by Lähdeniemi (**Supplemental figure 1.B.**). To test this theory, cells would have to be treated for a longer period and have their keratin levels measured; however, this could also lead to increased apoptosis.

7 CONCLUSIONS

In conclusion (**Figure 18.**), we show that K8 is protecting the colon epithelium and K8 deletion leads to a hyperactive PI3K/Akt/mTOR pathway. The activation enhances the translation of the hypoxia pathway's well established transcription factor, HIF-1α, which likely serves as a colonic protective factor. The increase of HIF-1α does not lead to a change in target genes VEGF and Bcl2, possibly due to suppressed DNA/coactivator binding. Moreover, HIF-1α was shown to be localized in a higher degree in the nucleus of *in vitro* and *ex vivo* K8 knockout models, which could be due to lost K8-HIF interaction. Lastly, we have determined that keratin levels (K8 and K19) are not upregulated *in vitro* during acute hypoxic stress. In the future, these results may help us develop a better understanding of the cellular events of colonic diseases.

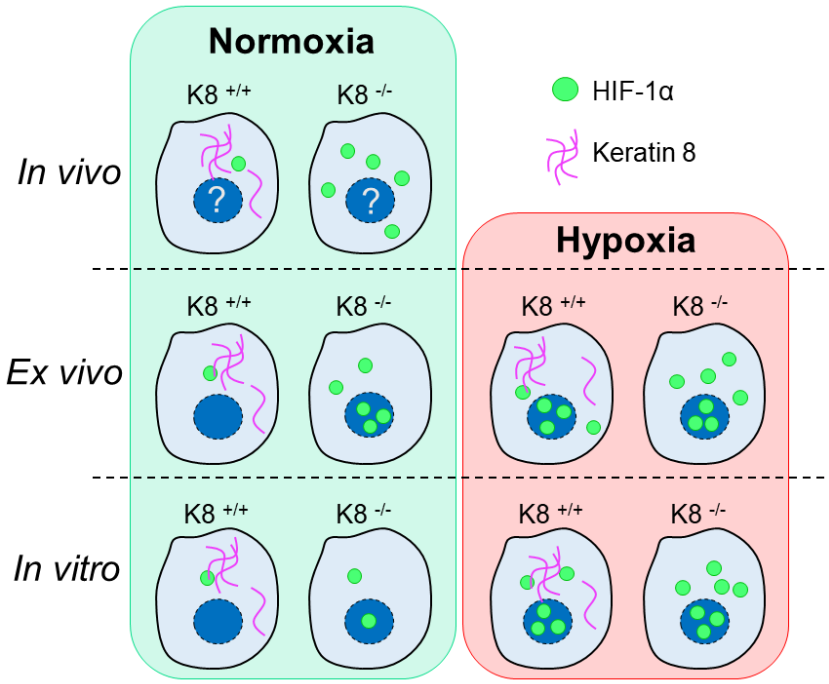

Figure 18. K8 deletion leads to increased HIF-1α, and higher *ex vivo* and *in vitro* nuclear translocation in normoxic conditions. All $K8^{-/-}$ models showed higher levels of HIF-1α (green dots) in normoxia and *ex vivo* and *in vitro* $K8^{-/-}$ models exhibited the same in hypoxic conditions. Furthermore, $K8^{-/-}$ *in vitro* and *ex vivo* models showed signs of higher HIF-1α nuclear levels in normoxia. Keratin (purple strands) levels in the *in vitro* $K8^{+/+}$ model were not upregulated in hypoxia.

8 SVENSK SAMMANFATTNING

STUDIE AV HUR K8 REGLERAR HYPOXISIGNALERINGEN I TJOCKTARMEN

8.1 Introduktion

Celler innehåller ett komplext nätverk av cytoskelettproteiner som ger dem strukturellt stöd samt hjälper cellerna i olika cellulära processer såsom rörelse och transport. Cytoskelettet är indelat i tre huvudgrupper, mikrofilament, mikrotubuli och intermediära filament. Intermediära filament är mycket flexibla, dynamiska och stabila proteiner som skapar filamentsträngar, som sträcker sig genom cytosolen och ansluter till andra cytoskelett (Omary, 2009; Fletcher, Mullins, 2010). De intermediära filamenten är indelade i sex grupper, som uttrycks cell- och vävnadsspecifikt. Denna avhandling fokuserar på typ I- och typ II- intermediära filament, det vill säga keratiner.

Tjocktarmen är sista delen i mag-tarmkanalen och har till uppgift att extrahera de kvarstående näringsämnena, vatten, vitaminer och mineraler ur tarmens innehåll. Det innersta lagret av tjocktarmen, epitelet, består av snabbt förnyande kryptor. Epitelet har som funktion att absorbera näringsämnen, producera slem, förmedla signaler, och tillsammans med tarmens bakteriella ekosystem skapar epitelet en vägg som försvarar oss mot patogener (Garrett, Gordon & Glimcher, 2010; Caballero, Finglas & Toldrá, 2015). Tjocktarmsepitelet är rikt på keratiner (Typ I: K15, K20, K23, K24, K18, K19 och Typ II: K8, K80) som skapar ett nätverk av byggnadsställningar och skyddar cellerna från mekanisk och kemisk stress, samt deltar i signalering och indelning av cytoplasmiska komponenter (Pallari, Eriksson, 2006; Polari et al., 2020). Keratinernas betydelse i tjocktarmen har visats i studier där förlusten av K8 hos möss orsakar hyperproliferation av epitelceller i tjocktarmen, kolit och diarré (Baribault et al., 1994; Habtezion et al., 2005). Dessutom utvecklar dessa $K8^{-/-}$-möss tumörer i tjocktarmen då de behandlas med cancerframkallande ämnen eller då de har en mutation i Apc-tumörsuppressorn (Misiorek et al., 2016).

I frånvaro av syre och/eller under påverkan av tillväxtfaktorer aktiveras hypoxisignaleringen. Generellt sett korrelerar aktiveringen av signaleringen med diverse patologiska tillstånd såsom hjärttillstånd och tumörtillväxt, men i vissa fall kan hypoxisignaleringen aktiveras även i icke-patologiska tillstånd, däribland högintensiv träning (Lundby, Gassmann & Pilegaard, 2006; Lee et al., 2019). Vid aktivering ökar translationen och stabiliseringen av den välkända transkriptionsfaktorn, HIF-1α. Stabiliserat HIF-1α binder och dimeriserar med sin partner ARNT som vidare binder till dess samfaktorer p300/CBP och aktiverar transkriptionen av ett hundratal gener. Proteinerna som är ett resultat av den transkriptionella aktiveringen arbetar tillsammans för att till exempel reglera ämnesomsättningen i syfte att undvika oxidativa skador, öka angiogenesen till det hypoxiska området samt öka mängden erytrocyter för att åstadkomma högre syreutbyte (Semenza, 2007).

Tidigare experiment i Diana Toivolas laboratorium har indikerat att K8 är involverad i regleringen av hypoxisignaleringen. Syftet med detta examensarbete var därför att utveckla en djupare förståelse av interaktionerna mellan K8 och hypoxisignaleringen, och undersöka vad K8 förlust resulterar i med avseende på signaleringen. Hypotesen var att K8 nedreglerar aktiverare uppströms från HIF-1α, vilket resulterar i lägre transkription av HIF-1α. Vid förlust av K8 tros halterna och nukleära translokaliseringen av HIF-1α öka. Vidare antas keratinhalterna öka i tjocktarmscancerceller när de utsätts för hypoxi.

I avhandlingen användes western blot-analys för att undersöka och mäta proteinhalter, kvantitativ PCR för att mäta mRNA-halter, immunofärgning för att undersöka lokalisering och slutligen kvantifiering och statistisk analys av erhållna resultat.

8.2 Resultat och diskussion

Lähdeniemi et al., (Manuskript) injicerade möss med en hypoximarkör och kom fram till at $K8^{-/-}$-möss hade en mera hypoxisk tarm (**Supplemental figur 1.A.**). I denna avhandling undersöktes därför hypoxisignaleringens transkriptionsfaktor HIF-1α och det framkom att transkriptionsfaktorn överuttrycks i våra $K8^{-/-}$ in vivo, in vitro och ex vivo-modeller (**Figur 10., 12.-13.**). För att bestämma effektiviteten av HIF-1α gjordes en kvantitativ PCR-analys på dess målgener men det visade sig att det inte fanns någon skillnad mellan $K8^{+/+}$- och $K8^{-/-}$-möss. Orsaken till detta är okänd men kunde förklaras av kromatinmodifieringar eller nedreglerad transkriptionell aktivering till exempel via $p14^{ARF}$ eller CITED2/CITED4 (Bárdos, Ashcroft, 2005; Horak et al., 2010). Med tanke på att HIF-1α har visats reglera ett hundratal gener, kunde det dessutom helt enkelt vara så att generna som undersöktes inte har en skillnad i uttryck medan andra har (Semenza, 2007). För att kunna uttala sig om HIF-1α:s aktivitet borde flera av HIF-1α målgener undersökas.

Resultaten (**Figur 11.**) tyder på att PI3K/Akt/mTOR-signaleringen är överaktiv, vilket är orsaken till den förhöjda halten HIF-1α. Studier har visat att K8 interagerar med Akt, vilket formade hypotesen att K8 fungerar som en ”fosfatsvamp” (eng. phosphate sponge) som kan ta åt sig de aktiverande fosforyleringarna av Akt, och således tysta PI3K/Akt/mTOR-signaleringen (**Figur 17.A.**) (Ku, Omary, 2006). Därmed skulle förlusten av K8 leda till en överaktiv PI3K/Akt/mTOR-signalering, i enlighet med resultaten. Vidare visades att den förhöjda halten av HIF-1α inte var ett resultat av inflammation (**Figur 11.**), men däremot har förlusten av K8 visats leda till förhöjda nivåer av cytokiner, vilket kunde vara en annan förklaring till den överaktiva PI3K/Akt/mTOR-signaleringen (**Figur 17.B.**) (Habtezion et al., 2005). Cytokiner aktiverar tyrosinkinasreceptorer (RTK), som i sin tur aktiverar signaleringsräckorna PI3K/Akt/mTOR och RAS/RAF/MEK/ERK som står för transkriptionen av HIF-1α. För att vidare komma till en slutsats med dessa hypoteser borde aktiviteten i RAS/RAF/MEK/ERK-signaleringen undersökas. Ifall även denna signalering visar sig vara aktiv i $K8^{-/-}$-möss, skulle det tyda

på att K8 fungerar som en stressdämpare och dess förlust leder till förhöjda cytokin halter och ett förhöjt uttryck av HIF-1α.

För att undersöka om K8 påverkar lokaliseringen av HIF-1α, immunofärgades K8 CRISPR/Cas9 celler samt organoider. Cellerna och organoiderna odlades i normoxi och hypoxi, varefter de färgades och mängden HIF-1α signal i kärnan av celler kvantifierades. Resultaten (**Figur 15.**) visade att HIF-1α är mera lokaliserat i kärnan i $K8^{-/-}$-modellerna i normoxi, men ingen skillnad upptäcktes vid hypoxi. Begränsningen med denna studie är att den förhöjda HIF-1α kärnlokaliseringen inte kan förklaras med säkerhet. Det kan vara ett resultat av den allmänt förhöjda nivån HIF-1α i $K8^{-/-}$-modeller, men även av en mer permeabel kärnmembran eller förlorad K8-HIF-1α kontakt (Stenvall et al., 2020).

Sammanfattningsvis (**Figur 18.**) visades i denna avhandling att K8-förlust leder till en överaktiv PI3K/Akt/mTOR signalering och förhöljda halter HIF-1α, som fungerar som en skyddsfaktor mot stress. Vidare visades det att HIF-1α är mer lokaliserat i kärnan av $K8^{-/-}$-modeller i normoxi, men den exakta mekanismen är fortfarande okänd.

9 ACKNOWLEDGEMENTS

First, I would like to acknowledge and give my warmest thanks to my supervisors Diana Toivola and Carl-Gustaf Stenvall. Thank you, Diana, for letting me work in your research lab and for your precious help in the process of completing my thesis. Thank you, Calle, for your excellent supervising, the joy you bring with you, and your perseverance helping me with this thesis. Because of you two, I have got the chance to develop valuable skills for my future career.

I would also like to sincerely thank all the members of Epithelial biology lab and all the lecturers of Åbo Akademi University. Lastly, I would like to thank my friends and family who have supported my way through university, especially my friends with whom I have worked with in BioCity along these years, I will forever cherish our memories.

Thank you all!

11 REFERENCES

Aherne, C.M., Saeedi, B., Collins, C.B., Masterson, J.C., McNamee, E.N., Perrenoud, L., Rapp, C.R., Curtis, V.F., Bayless, A. & Fletcher, A. 2015, "Epithelial-specific A2B adenosine receptor signaling protects the colonic epithelial barrier during acute colitis", *Mucosal immunology*, vol. 8, no. 6, pp. 1324-1338.

Azzouz, L.L. & Sharma, S. 2018, "Physiology, large intestine".

Bárdos, J.I. & Ashcroft, M. 2005, "Negative and positive regulation of HIF-1: a complex network", *Biochimica et Biophysica Acta (BBA)-Reviews on Cancer,* vol. 1755, no. 2, pp. 107-120.

Baribault, H., Penner, J., Iozzo, R.V. & Wilson-Heiner, M. 1994, "Colorectal hyperplasia and inflammation in keratin 8-deficient FVB/N mice.", *Genes & development,* vol. 8, no. 24, pp. 2964-2973.

Bragulla, H.H. & Homberger, D.G. 2009, "Structure and functions of keratin proteins in simple, stratified, keratinized and cornified epithelia", *Journal of anatomy,* vol. 214, no. 4, pp. 516-559.

Bustos-Fernández, L. 2013, *Colon: structure and function,* Springer Science & Business Media.

Caballero, B., Finglas, P. & Toldrá, F. 2015, *Encyclopedia of food and health,* Academic Press.

Cooper, G.M., Hausman, R.E. & Hausman, R.E. 2007, *The cell: a molecular approach,* ASM press Washington, DC.

Cortes, E., Lachowski, D., Robinson, B., Sarper, M., Teppo, J.S., Thorpe, S.D., Lieberthal, T.J., Iwamoto, K., Lee, D.A. & Okada-Hatakeyama, M. 2019, "Tamoxifen mechanically reprograms the tumor microenvironment via HIF-1A and reduces cancer cell survival", *EMBO reports,* vol. 20, no. 1, pp. e46557.

Coulombe, P.A. & Wong, P. 2004, "Cytoplasmic intermediate filaments revealed as dynamic and multipurpose scaffolds", *Nature cell biology,* vol. 6, no. 8, pp. 699-706.

Cummings, J.H. & Englyst, H.N. 1987, "Fermentation in the human large intestine and the available substrates", *The American Journal of Clinical Nutrition,* vol. 45, no. 5, pp. 1243-1255.

Escurat, M., Djabali, K., Gumpel, M., Gros, F. & Portier, M.M. 1990, "Differential expression of two neuronal intermediate-filament proteins, peripherin and the low-molecular-mass neurofilament protein (NF-L), during the development of the rat", *Journal of Neuroscience,* vol. 10, no. 3, pp. 764-784.

Fletcher, D.A. & Mullins, R.D. 2010, "Cell mechanics and the cytoskeleton", *Nature,* vol. 463, no. 7280, pp. 485-492.

Fuchs, E. 1983, "Evolution and complexity of the genes encoding the keratins of human epidermal cells", *Journal of Investigative Dermatology,* vol. 81, no. 1, pp. S141-S144.

Garrett, W.S., Gordon, J.I. & Glimcher, L.H. 2010, "Homeostasis and inflammation in the intestine", *Cell,* vol. 140, no. 6, pp. 859-870.

Garvin, S. & Dabrosin, C. 2003, "Tamoxifen inhibits secretion of vascular endothelial growth factor in breast cancer in vivo", *Cancer research,* vol. 63, no. 24, pp. 8742-8748.

Glover, L.E., Bowers, B.E., Saeedi, B., Ehrentraut, S.F., Campbell, E.L., Bayless, A.J., Dobrinskikh, E., Kendrick, A.A., Kelly, C.J. & Burgess, A. 2013, "Control of creatine metabolism by HIF is an endogenous mechanism of barrier regulation in colitis", *Proceedings of the National Academy of Sciences*, vol. 110, no. 49, pp. 19820-19825.

Gruenbaum, Y. & Foisner, R. 2015, "Lamins: nuclear intermediate filament proteins with fundamental functions in nuclear mechanics and genome regulation", *Annual Review of Biochemistry,* vol. 84, pp. 131-164.

Habtezion, A., Toivola, D.M., Asghar, M.N., Kronmal, G.S., Brooks, J.D., Butcher, E.C. & Omary, M.B. 2011, "Absence of keratin 8 confers a paradoxical microflora-dependent resistance to apoptosis in the colon", *Proceedings of the National Academy of Sciences,* vol. 108, no. 4, pp. 1445-1450.

Habtezion, A., Toivola, D.M., Butcher, E.C. & Omary, M.B. 2005a, "Keratin-8-deficient mice develop chronic spontaneous Th2 colitis amenable to antibiotic treatment", *Journal of cell science,* vol. 118, no. 9, pp. 1971-1980.

Heck, T., Vargas, D.A., Smeets, B., Ramon, H., Van Liedekerke, P. & Van Oosterwyck, H. 2020, "The role of actin protrusion dynamics in cell migration through a degradable viscoelastic extracellular matrix: Insights from a computational model", *PLoS computational biology,* vol. 16, no. 1, pp. e1007250.

Herrmann, H., Bär, H., Kreplak, L., Strelkov, S.V. & Aebi, U. 2007, "Intermediate filaments: from cell architecture to nanomechanics", *Nature reviews Molecular cell biology,* vol. 8, no. 7, pp. 562-573.

Horak, P., Crawford, A.R., Vadysirisack, D.D., Nash, Z.M., DeYoung, M.P., Sgroi, D. & Ellisen, L.W. 2010, "Negative feedback control of HIF-1 through REDD1-regulated ROS suppresses tumorigenesis", *Proceedings of the National Academy of Sciences,* vol. 107, no. 10, pp. 4675-4680.

Humphries, A. & Wright, N.A. 2008, "Colonic crypt organization and tumorigenesis", *Nature Reviews Cancer,* vol. 8, no. 6, pp. 415-424.

Jacob, J.T., Coulombe, P.A., Kwan, R. & Omary, M.B. 2018a, "Types I and II keratin intermediate filaments", *Cold Spring Harbor perspectives in biology,* vol. 10, no. 4, pp. a018275.

Karhausen, J., Furuta, G.T., Tomaszewski, J.E., Johnson, R.S., Colgan, S.P. & Haase, V.H. 2004, "Epithelial hypoxia-inducible factor-1 is protective in murine experimental colitis", *The Journal of clinical investigation,* vol. 114, no. 8, pp. 1098-1106.

Katsumoto, T., Mitsushima, A. & Kurimura, T. 1990, "The role of the vimentin intermediate filaments in rat 3Y1 cells elucidated by immunoelectron microscopy and computer-graphic reconstruction", *Biology of the Cell,* vol. 68, no. 1-3, pp. 139-146.

Kelly, C. J., Zheng, L., Campbell, E. L., Saeedi, B., Scholz, C. C., Bayless, A. J., Wilson, K.E., Glover, L.E., Kominsky, D.J., Magnuson, A., Weir, T.L., Ehrentraut, S.F., Pickel, C., Kuhn, K.A., Lanis, J.M., Nguyen, V., Taylor, C.T. & Colgan, S. P. (2015). Crosstalk between microbiota-derived short-chain fatty acids and intestinal epithelial HIF augments tissue barrier function. *Cell host & microbe*, vol. 17, no. 5, pp. 662-671.

Kirchberger, S., Royston, D.J., Boulard, O., Thornton, E., Franchini, F., Szabady, R.L., Harrison, O. & Powrie, F. 2013, "Innate lymphoid cells sustain colon cancer through production of interleukin-22 in a mouse model", *Journal of Experimental Medicine,* vol. 210, no. 5, pp. 917-931.

Ku, N. & Omary, M.B. 2006, "A disease-and phosphorylation-related nonmechanical function for keratin 8", *The Journal of cell biology*, vol. 174, no. 1, pp. 115-125.

Ku, N., Toivola, D.M., Strnad, P. & Omary, M.B. 2010, "Cytoskeletal keratin glycosylation protects epithelial tissue from injury", *Nature cell biology,* vol. 12, no. 9, pp. 876-885.

Lee, J.W., Ko, J., Ju, C. & Eltzschig, H.K. 2019, "Hypoxia signaling in human diseases and therapeutic targets", *Experimental & molecular medicine,* vol. 51, no. 6, pp. 1-13.

Leube, R.E. & Schwarz, N. 2016, "Intermediate filaments". *Encyclopedia of Cell Biology*, vol.2, pp. 569-578.

Li, H., Zhou, Y., Li, L., Li, S., Long, D., Chen, X., Zhang, J., Feng, L. & Li, Y. 2019, "HIF-1α protects against oxidative stress by directly targeting mitochondria", *Redox biology,* vol. 25, pp. 101109.

Liu, C., Lin, H., Tang, M. & Wang, Y. 2015, "Vimentin contributes to epithelial-mesenchymal transition cancer cell mechanics by mediating cytoskeletal organization and focal adhesion maturation", *Oncotarget,* vol. 6, no. 18, pp. 15966.

Lundby, C., Gassmann, M. & Pilegaard, H. 2006, "Regular endurance training reduces the exercise induced HIF-1α and HIF-2α mRNA expression in human skeletal muscle in normoxic conditions", *European journal of applied physiology,* vol. 96, no. 4, pp. 363-369.

Lähdeniemi, I.K.A., Stenvall, C.A., Miikkulainen, P., Ghimire, A., Weckström, F., Heikkilä, T., Mairinoja, L.P., Helenius, T.O., Grönroos, T., Silvander, J.S.G., Ridge, K.M., Jaakkola, P., Toivola, D.M. 2021, “Keratins are upregulated during hypoxia and modulate the hypoxia signaling pathway in colonic epithelia”. Manuscript.

Macfarlane, G.T. & Macfarlane, S. 2012, "Bacteria, colonic fermentation, and gastrointestinal health", *Journal of AOAC International,* vol. 95, no. 1, pp. 50-60.

Macfarlane, G.T. & Macfarlane, S. 2011, "Fermentation in the human large intestine: its physiologic consequences and the potential contribution of prebiotics", *Journal of clinical gastroenterology,* vol. 45, pp. S120-S127.

Masoud, G.N. & Li, W. 2015, "HIF-1α pathway: role, regulation and intervention for cancer therapy", *Acta Pharmaceutica Sinica B,* vol. 5, no. 5, pp. 378-389.

Mescher, A.L. 2013, *Junqueira's basic histology: text and atlas,* McGraw-Hill Medical 13th ed. New York.

Michalczyk, K. & Ziman, M. 2005, "Nestin structure and predicted function in cellular cytoskeletal organisation", *Histology and histopathology,* vol. 20, no.2.

Misiorek, J.O., Lähdeniemi, I.A., Nyström, J.H., Paramonov, V.M., Gullmets, J.A., Saarento, H., Rivero-Müller, A., Husøy, T., Taimen, P. & Toivola, D.M. 2016, "Keratin 8-deletion induced colitis predisposes to murine colorectal cancer enforced by the inflammasome and IL-22 pathway", *Carcinogenesis,* vol. 37, no. 8, pp. 777-786.

Mohyeldin, A., Garzón-Muvdi, T., & Quiñones-Hinojosa, A. (2010). “Oxygen in stem cell biology: a critical component of the stem cell niche”, *Cell stem cell*, vol. 7, no. 2, pp. 150-161.

Moll, R., Divo, M. & Langbein, L. 2008, "The human keratins: biology and pathology", *Histochemistry and cell biology,* vol. 129, no. 6, pp. 705.

Nigam, Y., Knight, J. & Williams, N. 2019, "Gastrointestinal tract 5: the anatomy and functions of the large intestine", *Nursing times,* vol. 115, no. 10, pp. 50-53.

Nogales, E. 2001, "Structural insights into microtubule function", *Annual Review of Biophysics and Biomolecular Structure,* vol. 30, no. 1, pp. 397-420.

Omary, M.B. 2009, "“IF-pathies”: a broad spectrum of intermediate filament–associated diseases", *The Journal of clinical investigation,* vol. 119, no. 7, pp. 1756-1762.

Omary, M.B., Coulombe, P.A. & McLean, W.I. 2004, "Intermediate filament proteins and their associated diseases", *New England Journal of Medicine,* vol. 351, no. 20, pp. 2087-2100.

Omary, M.B., Ku, N., Tao, G., Toivola, D.M. & Liao, J. 2006, "‘Heads and tails’ of intermediate filament phosphorylation: multiple sites and functional insights", *Trends in biochemical sciences,* vol. 31, no. 7, pp. 383-394.

Pallari, H. & Eriksson, J.E. 2006, "Intermediate filaments as signaling platforms", *Science's STKE,* vol. 2006, no. 366, pp. pe53.

Polari, L., Alam, C.M., Nyström, J.H., Heikkilä, T., Tayyab, M., Baghestani, S. & Toivola, D.M. 2020, "Keratin intermediate filaments in the colon: Guardians of epithelial homeostasis", *The international journal of biochemistry & cell biology,* vol. 129, pp. 105878.

Poon, E., Howman, E.V., Newey, S.E. & Davies, K.E. 2002, "Association of syncoilin and desmin: linking intermediate filament proteins to the dystrophin-associated protein complex", *Journal of Biological Chemistry,* vol. 277, no. 5, pp. 3433-3439.

Russell, M.A. 2020, "Synemin Redefined: Multiple Binding Partners Results in Multifunctionality", *Frontiers in cell and developmental biology,* vol. 8, pp. 159.

Saeedi, B.J., Kao, D.J., Kitzenberg, D.A., Dobrinskikh, E., Schwisow, K.D., Masterson, J.C., Kendrick, A.A., Kelly, C.J., Bayless, A.J. & Kominsky, D.J. 2015, "HIF-dependent regulation of claudin-1 is central to intestinal epithelial tight junction integrity", *Molecular biology of the cell*, vol. 26, no. 12, pp. 2252-2262.

Schödel, J., Mole, D.R. & Ratcliffe, P.J. 2013, "Pan-genomic binding of hypoxia-inducible transcription factors", *Biological chemistry,* vol. 394, no. 4, pp. 507-517.

Semenza, G.L. 2007, "Hypoxia-inducible factor 1 (HIF-1) pathway", *Science's STKE,* vol. 2007, no. 407, pp. cm8.

Shah, Y.M. 2016, "The role of hypoxia in intestinal inflammation", *Molecular and cellular pediatrics,* vol. 3, no. 1, pp. 1-5.

Shiels, A. & Hejtmancik, J.F. 2015, "Molecular genetics of cataract", *Progress in molecular biology and translational science,* vol. 134, pp. 203-218.

Singhal, R. & Shah, Y.M. 2020, "Oxygen battle in the gut: Hypoxia and hypoxia-inducible factors in metabolic and inflammatory responses in the intestine", *Journal of Biological Chemistry*, vol. 295, no. 30, pp. 10493-10505.

Snider, N.T. & Omary, M.B. 2014, "Post-translational modifications of intermediate filament proteins: mechanisms and functions", *Nature reviews Molecular cell biology,* vol. 15, no. 3, pp. 163-177.

Stenvall, C.A., Nyström, J.H., Butler-Hallissey, C., Adam, S.A., Foisner, R., Ridge, K.M., Goldman, R.D. & Toivola, D.M. 2020, "Keratins couple with the nuclear lamina and regulate proliferation in colonic epithelial cells", *bioRxiv*.

Stenvall, C.A., Tayyab, M., Grönroos, T.J, Ilomäki, M.A., Viiri, K., Ridge, K.M., Polari, L., Toivola, D.M. 2021, “Targeted deletion of keratin 8 in intestinal epithelial cells disrupts tissue integrity and predisposes to tumorigenesis in the colon”. *Cellular and Molecular Life Sciences*, vol. 79, no. 1, pp. 1-17.

Synnestvedt, K., Furuta, G.T., Comerford, K.M., Louis, N., Karhausen, J., Eltzschig, H.K., Hansen, K.R., Thompson, L.F. & Colgan, S.P. 2002, "Ecto-5′-nucleotidase (CD73) regulation by hypoxia-inducible factor-1 mediates permeability changes in intestinal epithelia", *The Journal of clinical investigation*, vol. 110, no. 7, pp. 993-1002.

Szmulowicz, U.M. & Hull, T.L. 2011, "Colonic physiology" in *The ASCRS textbook of colon and rectal surgery* Springer, pp. 23-39.

Toivola, D.M., Strnad, P., Habtezion, A. & Omary, M.B. 2010, "Intermediate filaments take the heat as stress proteins", *Trends in cell biology,* vol. 20, no. 2, pp. 79-91.

Toivola, D.M., Boor, P., Alam, C. & Strnad, P. 2015, "Keratins in health and disease", *Current opinion in cell biology,* vol. 32, pp. 73-81.

Toivola, D.M., Krishnan, S., Binder, H.J., Singh, S.K. & Omary, M.B. 2004, "Keratins modulate colonocyte electrolyte transport via protein mistargeting", *The Journal of cell biology,* vol. 164, no. 6, pp. 911-921.

Toivola, D.M., Tao, G., Habtezion, A., Liao, J. & Omary, M.B. 2005, "Cellular integrity plus: organelle-related and protein-targeting functions of intermediate filaments", *Trends in cell biology,* vol. 15, no. 11, pp. 608-617.

Troy, C.M., Muma, N.A., Greene, L.A., Price, D.L. & Shelanski, M.L. 1990, "Regulation of peripherin and neurofilament expression in regenerating rat motor neurons", *Brain research,* vol. 529, no. 1-2, pp. 232-238.

Viedma-Poyatos, Á, Pajares, M.A. & Pérez-Sala, D. 2020, "Type III intermediate filaments as targets and effectors of electrophiles and oxidants", *Redox biology,* vol. 36, pp. 101582.

Xue, X., Ramakrishnan, S., Anderson, E., Taylor, M., Zimmermann, E.M., Spence, J.R., Huang, S., Greenson, J.K. & Shah, Y.M. 2013, "Endothelial PAS domain protein 1 activates the inflammatory response in the intestinal epithelium to promote colitis in mice", *Gastroenterology,* vol. 145, no. 4, pp. 831-841.

Yang, J., AlTahan, A., Jones, D.T., Buffa, F.M., Bridges, E., Interiano, R.B., Qu, C., Vogt, N., Li, J. & Baban, D. 2015, "Estrogen receptor-α directly regulates the hypoxia-inducible factor 1 pathway associated with antiestrogen response in breast cancer", *Proceedings of the National Academy of Sciences,* vol. 112, no. 49, pp. 15172-15177.

Zhao, J. & Liem, R.K. 2016, "α-internexin and peripherin: expression, assembly, functions, and roles in disease", *Methods in enzymology,* vol. 568, pp. 477-507.

Ziello, J.E., Jovin, I.S. & Huang, Y. 2007, "Hypoxia-Inducible Factor (HIF)-1 regulatory pathway and its potential for therapeutic intervention in malignancy and ischemia", *The Yale journal of biology and medicine,* vol. 80, no. 2, pp. 51.

11 APPENDIX

11.1 Supplemental figures

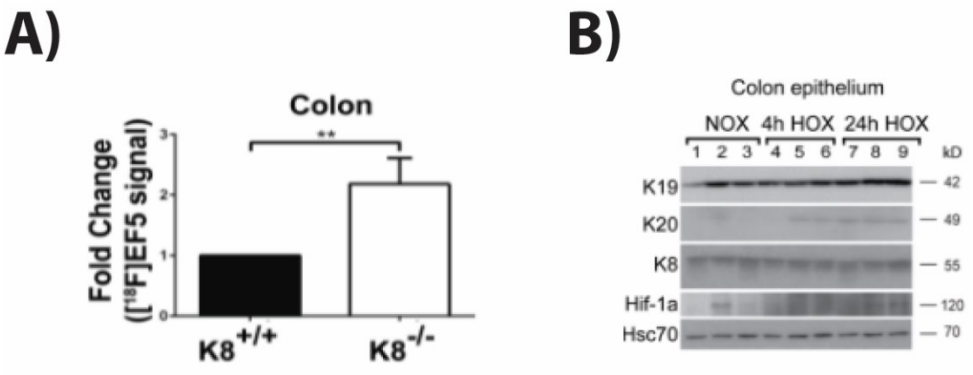

Supplemental figure 1. Increased hypoxia in colon of K8 $^{-/-}$ mice and increase in K19 and K20 after hypoxia treatment. (A) The uptake of the hypoxia-tracer [^{18}F] EF5 in the colon and fold change between K8 $^{+/+}$ and K8 $^{-/-}$ mice. **(B)** Western blot of keratin (K19, K20 and K8) after hypoxia treatment (4h wells 4-6 and 24h wells 7-9) (n=3). An upregulation was observed for K19 and K20 (Lähdeniemi et al., Manuscript). ** = $p<0.01$.

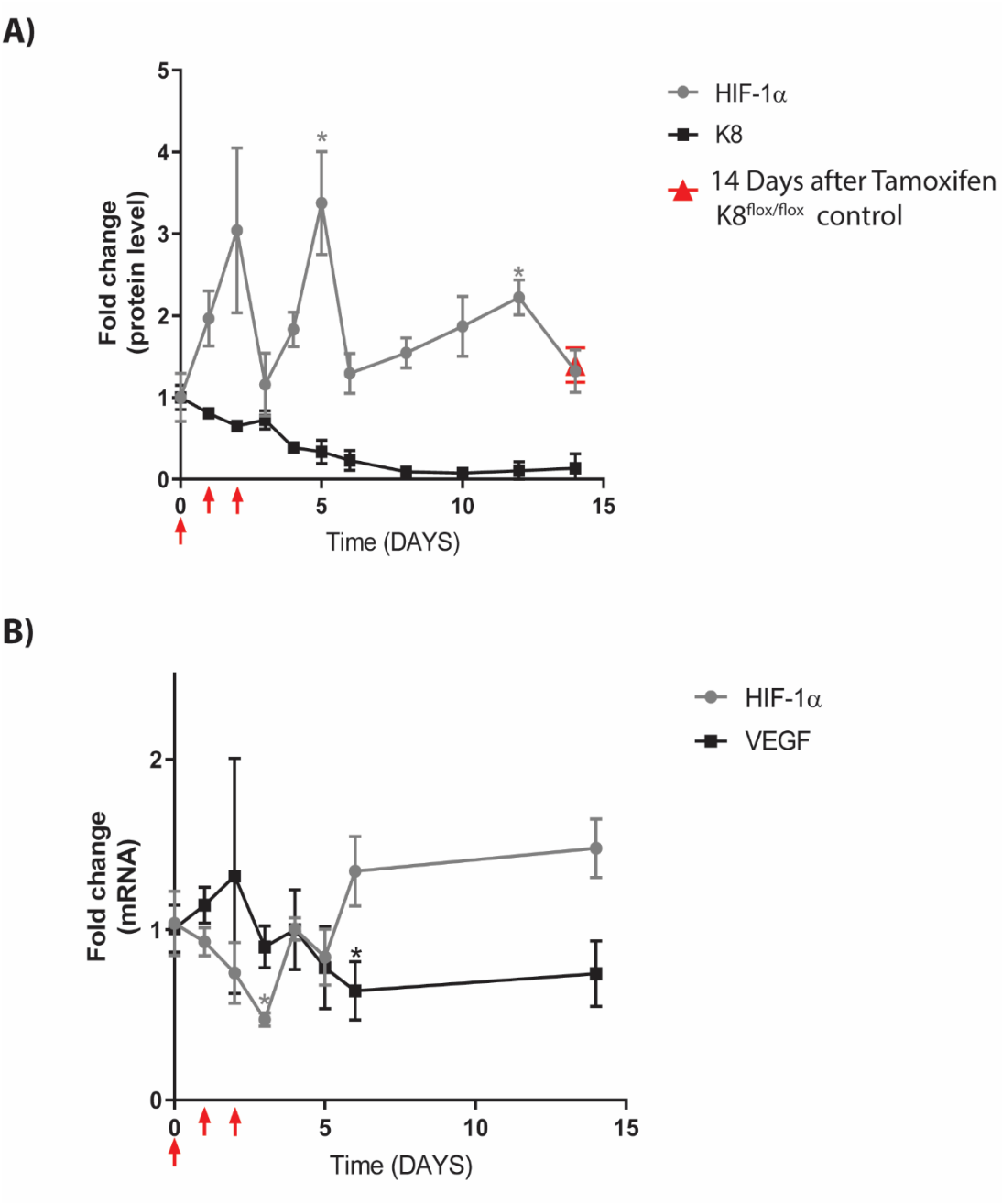

Supplemental figure 2. K8 knockout time-course experiment influenced by Tamoxifen. (**A**) $K8^{flox/flox}$; Villin-$CreER^{t2}$ mice were injected day 0, 1 and 2 (red arrows) with tamoxifen and 3 mice per time point were sacrificed. Their protein levels of HIF-1α and K8 were measured from colon total lysates and normalized to β-tubulin. (**B**) Time course illustrating mRNA levels (HIF-1α and VEGF) from the colon total lysates of the same mice. Statistical significance was calculated with student's t-test where * = $p<0.05$.

11.2 Buffers and recipes

3 x Laemmli buffer	
100% Glycerol (Calbiochem)	30 ml
20% SDS	15 ml
6,625 M Tris-HCL pH 6.8 (Merck)	30 ml
0,15% bromophenol blue (Merck)	10 ml
MQ-H_2O	12 ml
300 µl ß-mercaptoethanol (Sigma Aldrich) is added to 9,7 ml of 3 x Laemmli buffer before use	

20% SDS	
SDS (Thermo Fisher)	20 g
dH_2O	100 ml

1 x PBS
1 x PBS tablet (Mediago) diluted in 1 liter of dH_2O

Lower gel stock	
Trizma-Base (1,5 M)(Sigma)	90.75 g
Trizma-Base is diluted in 100 ml dH_20, pH is set to 8.8 and it is further diluted to 500 ml with dH_20	

10 x Running buffer	
Trizma-Base (1,5 M)	60 g
Glycine (Sigma Aldrich)	288 g
Trizma-base and glycine is dissolved in 500 ml dH_2O, whereafter diluted to 2 liters with dH_20	

Stacking gel (2 gels)	
Upper gel stock	1.25 ml
Acrylamide (Sigma Aldrich)	0.75 ml
20% SDS	0.05 ml
MQ-H2O	3 ml
10% APS	0.02 ml
TEMED (Thermo Fisher)	0.01 ml

Running buffer (2 gels)	
10 x Running buffer	70 ml
MQ-H2O	to 700 ml
20% SDS	5 ml

Homogenization buffer	
SDS (Thermo Fisher)	6 g
EDTA (Merck)	2 ml
1,87 M Tris-HCL (Merck)	20 ml
Dissolved in 100 ml dH_2O, pH is set to 6.8 and diluted to 200 ml with dH_2O	

TEG buffer
20mM Tris-HCL pH 7.5
1mM EDTA
10% Glycerol

Lila Lysis buffer
25 mM Hepes pH 8
100 mM NaCl
5 mM EDTA pH 8
0.5% Triton X-100
20 mM Beta-glycerophosphate
20 mM Para-nitro-phenyl phosphate
100 µM Ortovanadate

Upper gel stock	
Trizma-Base (0,5 M) (Sigma Life Science)	30.25 g
Trizma-Base is dissolved in 100 ml dH_20, pH is set to 6.8 and diluted to 500 ml with dH_2O	

Running gel 10 % (2 gels)	
Lower gel stock	2.25 ml
Acrylamide (Sigma Aldrich)	3 ml
20% SDS	0.045 ml
MQ-H_2O	3.75 ml
10 % APS	0.06 ml
TEMED (Thermo Fisher)	0.006 ml

Transfer buffer (2 gels)	
10 x Running buffer	80 ml
MQ-H_2O	to 800 ml
20 % SDS	5 ml
Methanol	200 ml